Proton Production in Neutrino-Neon Collisions in the 15-ft. Bubble Chamber at the Tevatron

Mary A. Lauko

May 1993

THE STATE UNIVERSITY OF NEW JERSEY

RUTGERS

Department of Physics and Astronomy, P.O. Box 849, Piscataway, New Jersey 08855-0849

Proton Production in Neutrino-Neon Collisions in the 15 ft. Bubble Chamber at the Tevatron

by Mary A. Lauko

A dissertation submitted to the

Graduate School— New Brunswick

Rutgers, The State University of New Jersey

in partial fulfillment of the requirements

for the degree of

Doctor of Philosophy

Graduate Program in Physics

Written under the direction of

Dr. Mohan S. Kalelkar

and approved by

Mohan S. Kalelkar

Charles Glashausser

Peter Stamer

William M. Kloet

New Brunswick, New Jersey

May, 1993

ABSTRACT OF THE DISSERTATION

Proton Production in Neutrino-Neon Collisions in the 15 ft. Bubble Chamber at the Tevatron

by Mary A. Lauko, Ph.D.

Dissertation Director: Dr. Mohan S. Kalelkar

Proton production was studied in $\nu - {}^{20}Ne$ interactions in the 15 ft. Bubble Chamber at Fermilab, and the results were used to test models of the intranuclear cascade. The Bubble Chamber was filled with a heavy Ne-H_2 mixture, and was exposed to the wide-band Quadrupole Triplet neutrino beam produced by 800 GeV protons from the Tevatron. The data sample consisted of 8489 events, with a mean energy of 150 GeV, the highest energy at which neutrino interactions have ever been studied.

It is shown that "gray" protons, which are in the momentum range $0.3 - 1.2$ GeV/c, are the relevant ones for investigating nuclear effects. Neutrino events are measured to have a net charge excess of 0.39 ± 0.02 over what would be expected if there were no nuclear effects. It is found that the fully corrected excess of gray protons is 0.34 ± 0.02, which accounts for most or all of the charge excess. The mean net charge of events increases linearly with the number of gray protons, with a slope of 0.73 ± 0.03 as expected if the charge excess consists of gray protons. The fractional distribution of gray protons agrees with the model of Andersson, Otterlund and Stenlund, and is not consistent with a Poisson distribution. It is shown for the first time that gray proton production decreases with the total hadronic effective mass, corroborating the model that it is mostly low-energy particles that undergo rescattering.

A significant 19% of the gray protons are in the backward hemisphere with respect to the neutrino direction, which is kinematically forbidden in the absence of nuclear effects. Backward proton multiplicity is observed to increase linearly with forward multiplicity. It is shown for the first time that neutrino interactions are consistent with models that explain backward protons as originating from pion absorption, specifically the mechanisms: $\pi + \text{"}b\text{"} \rightarrow N + N$ and $\pi + \text{"}b\text{"} \rightarrow \Delta + N$ with $\Delta \rightarrow \pi + N$, where "b" is a two-nucleon cluster within the nucleus. It is also shown that the data do not convincingly corroborate the two-nucleon correlation model, which assumes direct interaction of the neutrino with the nuclear cluster.

Acknowledgements

This thesis has been made possible through the hard work and dedication of many people. My thesis advisor, Dr. Mohan Kalelkar, was very helpful in discussing physics aspects and programming difficulties. Dr. Peter Stamer was the coach who helped me through some years of film processing, and had the patience to pay attention to all the details of the experiment including the physics analysis. Dr. Richard Plano and my fellow graduate student Douglas DeProspo, who now has his Ph.D., set up the data reduction program chain which we used extensively to process the data. Among the local technical staff, Pieter Jacques maintained the online programs for running the measuring machines. John Doroshenko, who is now my husband, repaired the scanning and measuring equipment and kept the computers running at all hours of the day and night. The dedicated scanners at Rutgers were Julia Sotory, Amos Danube, Dorothy Horzepa, Doris Thomas and many part time college students. Thanks is also owed to the technical staff at Fermilab, including the staff operating the Bubble Chamber.

Dedication

This thesis is dedicated to my husband John Doroshenko for all his help and encouragement, and to my son Andrew who was born on October 3, 1992.

Table of Contents

Abstract ii

Acknowledgements iv

Dedication v

List of Tables vii

List of Figures viii

1. Introduction 1

2. Models of Nuclear Effects 5

2.1. Introduction 5

2.2. Intranuclear Cascade 5

2.3. Backward Proton Production 9

3. Experimental Description and Apparatus 13

3.1. Introduction 13

3.2. Beamline 13

3.3. 15 ft. Bubble Chamber 15

3.4. EMI-IPF 18

4. Data Collection and Reduction 21

4.1. Scanning 21

4.2. Measuring 22

4.3. Scanning/Measuring Difficulties 22

4.4. Data Reduction 23

4.5. Proton Flagging 24

5. Data Sample Selection 26

5.1. Selection of Charged Current and Neutral Current events 26

5.2. Energy Correction for Charged Current Events 26

5.3. Separation of Black and Gray Protons 27

5.4. Backward Proton Selection 33

6. Physics Results 34

6.1. Intranuclear Cascade in $\nu_\mu - Ne$ Charged Current Interactions 34

6.1.1. Net Charge Excess 34

6.1.2. Proton Excess 35

6.1.3. Weights for Protons 36

6.1.4. Results of Intranuclear Cascade Analysis 37

6.2. Backward Particle Production and the Rescattering Model 43

6.3. Pion Absorption 46

6.3.1. Evidence for $\pi + "b" \rightarrow N + N$ Mechanism 49

6.3.2. Evidence for $\pi + "b" \rightarrow \Delta + N$ Mechanism 51

6.4. The Two-Nucleon Correlation Model 57

6.5. Backward Particle Differential Cross Section 64

7. Conclusions 71

Appendix A. (νn) to (νp) Cross Section Ratio 74

References 76

Vita 77

List of Tables

4.1. Number of gray protons in each flag category 25

5.1. Minimum bias event sample 26

5.2. Gray proton multiplicity 29

5.3. Forward/backward gray proton multiplicity in all events 33

6.1. Mean multiplicities 34

6.2. Gray proton interaction lenghts in '85 film 37

6.3. Average gray proton multiplicity vs. Q^2 43

6.4. Average gray proton multiplicity vs. W^2 43

6.5. Delta resonances 56

6.6. $B(\theta)$ slope parameter 64

List of Figures

2.1. Quark diagrams of (a) CC and (b) $C\bar{C}$ interactions 6

2.2. Quark diagrams of NC interactions 7

3.1. Layout of the beamline at Fermilab(not to scale) 14

3.2. Side view of the 15 ft. Bubble Chamber 16

3.3. a) Top view of the IPF and the EMI planes. b) The arrangement of the three coordinates of the EMIB. 19

5.1. Bubble Chamber coordinate system 28

5.2. $\cos(\beta)$ for protons with $p < 300$ MeV/c 30

5.3. $\cos(\beta)$ for protons with $p \geq 300$ MeV/c 31

5.4. Momentum distribution of all protons 32

6.1. Interaction weight for gray protons 38

6.2. Plot of the radius of leaving tracks 39

6.3. Charge excess of an event versus the number of gray protons in the event 41

6.4. Fraction of events versus the number of gray protons in the events . . . 42

6.5. Mean energy per hadron (not including black protons) vs. Q^2 per event 44

6.6. Mean energy per hadron (not inluding black protons) vs. W^2 per event 45

6.7. Mean backward gray proton multiplicity versus forward gray proton multiplicity 47

6.8. Ratio of negative pion multiplicity to positive pion multiplicity in pion momentum bins. The solid curve shows the shape of the $\pi^+ d \rightarrow pp$ cross section 48

6.9. μ^2 for events with at least one backward proton. The solid line shows a polynomial fit to the background. 50

6.10. $M(p\pi^+)$ using backward pion with any gray proton 52

6.11. $M(p\pi^-)$ using backward pion with any gray proton 53

6.12. $M(p\pi^+)$ using backward pion with backward gray proton 54

6.13. $M(p\pi^-)$ using backward pion with backward gray proton 55

6.14. μ_1^2 using only backward pions which result in a Δ signal. The solid line shows a polynomial fit to the background. 58

6.15. $\mu_1^2 - \mu^2$ (see equation (6.5)) using only backward pions which result in Δ signal. 59

6.16. μ^2 for events with at least one backward proton and no backward pions. The solid line shows a polynomial fit to the background. 60

6.17. μ^2 for events with at least one backward proton and at least one backward pion. The solid line shows a polynomial fit to the background. . . 61

6.18. v_N vs. α for all events with at least one backward proton. The solid line shows the prediction of the SRO model. 62

6.19. v_N vs. α for all events with only one backward proton and no other gray protons. The solid line shows the prediction of the SRO model. . . 63

6.20. Differential distribution for backward protons 65

6.21. Differential distribution for backward protons in cases where the event contains only one backward proton and no other gray protons . . . 66

6.22. Differential distribution for backward π^+ 67

6.23. Differential distribution for backward π^- 68

6.24. $B(\theta)$ vs. E_{HAD} 70

Chapter 1

Introduction

The interactions of high-energy hadrons with nuclei have been studied in many experiments. The principal results have been summarized in Refs.[1, 2]. They provide a guide to the literature. The interaction process can be described as the projectile interacting with a nucleon in the nucleus, producing some particles, and causing the nucleon to recoil. While the projectile generally remains intact, it proceeds through the nucleus, undergoing successive collisions with additional nucleons. Also, there can be secondary collisions within the nucleus induced by the particles produced by the projectile collisions, or by the recoiling nucleons, generating an intranuclear cascade. The major consequence is that the net charge of all the particles in the final state is considerably greater than what can be expected based on charge conservation in the initial hadron-nucleon collision.

In hadron-nucleus experiments the rescattering of recoiling nucleons was found to contribute much more to the intranuclear cascade than the rescattering of particles produced by the successive projectile collisions. The reason is believed to be that in the projectile collisions the time scale for producing hadrons is of order 10^{-23} seconds, while in the rest frame of the relativistic hadron the nucleus is a highly Lorentz-contracted disk that passes by in a time less than this. Therefore such relativistic particles cannot rescatter, because they are produced outside the nucleus. On the other hand, recoiling nucleons are generally non-relativistic and may rescatter. Thus the study of protons in the final state is important in understanding the space-time development of the strong interactions[3].

One difficulty with hadron-nucleus experiments is that the charge excess in the final state is partly due to the multiple interactions of the projectile, and partly to

the rescattering of recoiling nucleons. It is not easy to separate these two sources of multiparticle production.

By contrast, neutrino-nucleus interactions have the advantage that the projectile neutrino interacts only once. When the neutrino interacts with a nucleon, it produces either a muon (in a charge-current interaction) or remains a neutrino (in a neutral-current interaction). Neither the muon nor the neutrino reinteracts in the nucleus. Therefore, any charge excess must be due to secondary collisions, thereby greatly easing the interpretation of the process. There are far fewer studies of the intranuclear cascade using neutrino projectiles [4, 5, 6, 7, 8] than hadron projectiles.

In this thesis we report a study of proton production by high energy neutrino interactions in neon nuclei, in order to investigate the nature of the intranuclear cascade, and to test theoretical models of the cascade. Our experiment was Fermilab experiment E632, and was performed at the Tevatron using the Fermilab horn-focussed wide-band neutrino beam targeted at the 15 ft. Bubble Chamber filled with a heavy mixture of Ne-H_2. This was the highest neutrino experiment to date, with an average neutrino event energy of 150 GeV. The experiment was conducted by a collaboration of 16 different labs:

1. University of California, Berkeley, CA 94720
2. University of Birmingham, Birmingham B15 2TT, U.K.
3. Inter-University Inst. for High Energies, B-1050 Brussels, Belgium
4. CERN, Ch-1211 Geneva 23, Switzerland
5. Panjab University, Chandigarh 160014, India
6. Fermilab, Batavia, IL 60510
7. University of Hawaii, Honolulu, HI 96822
8. Imperial College, London SW7 2AX, U.K.
9. Illinois Institute of Technology, Chicago, IL 60616

10. University of Jammu, Jammu 180001, India

11. Max-Planck-Institut fur Physik, D-8000 Munchen 40, Germany

12. Oxford University, Oxford OX1 3RH, U.K.

13. Rutgers University, New Brunswick, NJ 08903

14. CEN Saclay, F-91191 Gif-sur-Yvette CEDEX, France

15. Stevens Institute of Technology, Hoboken, NJ 07030

16. Tufts University, Medford, MA 02155

Sometime after the experiment was finished the collaboration was joined by three Russian groups to help with the scanning and measuring of the film.

1. IHEP Serpukhov, 142284 Protvino Moscow region, Russia

2. ITEP, 117259 Moscow, Russia

3. Moscow State University, 177234 Moscow, Russia

One problem with the study of proton production is common to both hadron and neutrino interactions. In both cases, the interactions of the projectiles can be expected to leave the nucleus in excited states, and the low-energy protons in the final state may be associated with the final evaporation of the nucleus. Such protons are referred to as "black" protons in the literature. Higher-energy protons, which really come from the cascade, are called "gray" protons. Models of nuclear effects, which are discussed in Chapter 2, require a study of gray protons. In Chapter 5 we explain how we can experimentally distinguish black and gray protons.

A significant portion of the gray proton sample is produced backward relative to the neutrino beam. In the literature they are called backward or cumulative particles. Such particles have been a source of interest, because they cannot be produced by a nucleon colliding with a single nucleon target. Either the target mass has to be increased or the target nucleon has to have some initial backward momentum which is balanced by the other nucleons. The second possibility is discussed in Ref.[9]. The models for

increasing the target mass assume some clustering of nucleons inside the nucleus; the names: short range order (SRO), or two nucleon correlation model both relate to the same principal idea. Among the mechanisms proposed for such clustering have been nuclear density fluctuations[10], two or three nucleon clusters with greater than average nucleon binding[11] and multiquark bags[12, 13]. It is also possible that an effective clustering of nucleons is produced by a combination of such mechanisms. Backward proton production has been studied in high energy experiments in Refs. [4, 5, 7, 6, 14].

In this thesis we will discuss the models of proton production in Chapter 2. Chapter 3 will discuss the details of the experiment including the description of the apparatus, while Chapter 4 will describe the data collection and reduction. The data selection will be explained in Chapter 5, and the physics analysis of the data will take place in Chapter 6. Conclusions will be drawn in Chapter 7.

Chapter 2

Models of Nuclear Effects

2.1 Introduction

The E632 experiment was performed using a wide band muon neutrino beam which collided with the Neon liquid inside the 15 ft. Bubble Chamber. Hence the possible interactions are:

$$\nu_\mu + Ne \rightarrow \mu^- + hadrons\ (CC) \tag{2.1}$$

$$\bar{\nu}_\mu + Ne \rightarrow \mu^+ + hadrons\ (C\bar{C}) \tag{2.2}$$

$$\nu_\mu + Ne \rightarrow \nu_\mu + hadrons\ (NC) \tag{2.3}$$

$$\bar{\nu}_\mu + Ne \rightarrow \bar{\nu}_\mu + hadrons\ (NC) \tag{2.4}$$

The mediating particle in the first two reactions is the $W^\pm$, in the last two is the Z^0. See Figures 2.1a, 2.1b, 2.2a and 2.2b corresponding to interactions (2.1),(2.2),(2.3) and (2.4), respectively. The above reactions are studied in this paper. The beam had a small electron neutrino component of approximately 3% for which similar interactions can be written, however, those are not studied here.

2.2 Intranuclear Cascade

There have been many studies of hadron-nucleus collisions[2] in which several projectile collisions ν can take place within the target nucleus as the original hadron passes through it. The number of such collisions is usually found using the observed gray proton multiplicity in the event (300 MeV/c $\leq p_{gray} \leq$ 1200 MeV/c, see section 5.3). However, the recoiling nucleons from each projectile collision pass through the nucleus colliding with other nucleons and often creating a cascade of gray protons. The effort

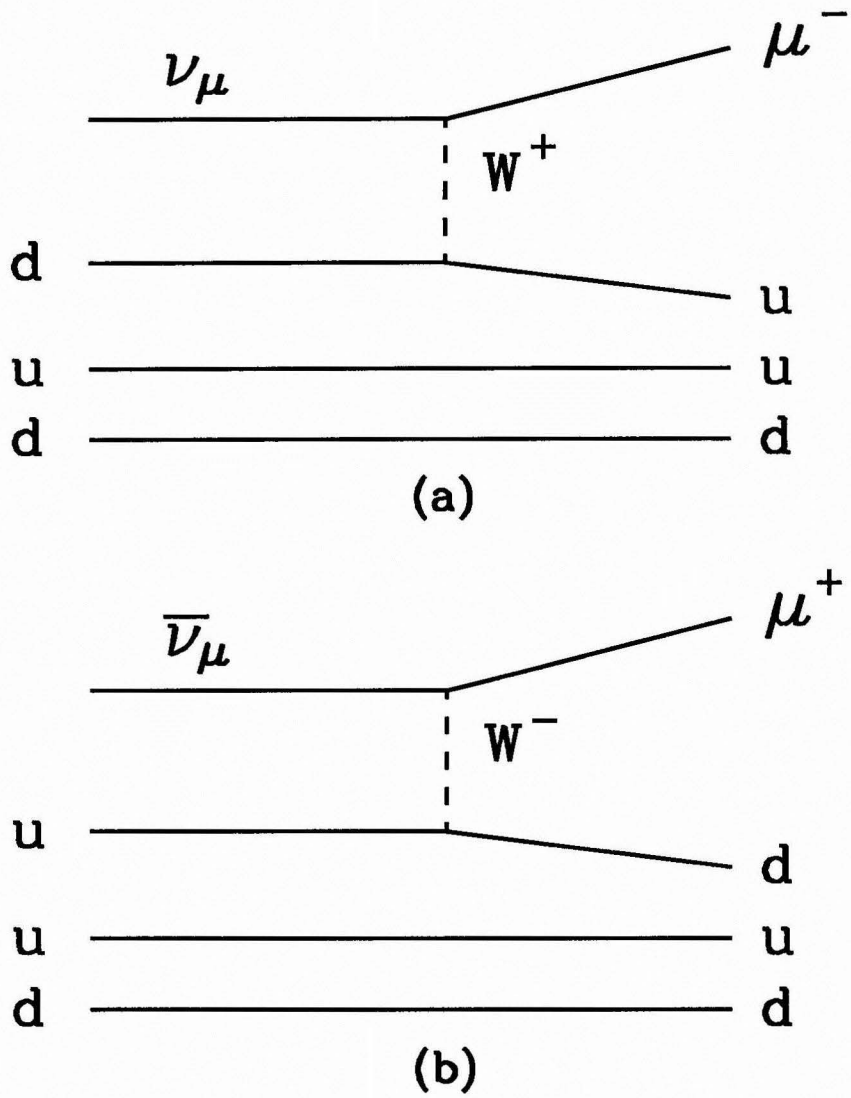

Figure 2.1: Quark diagrams of (a) CC and (b) $C\bar{C}$ interactions

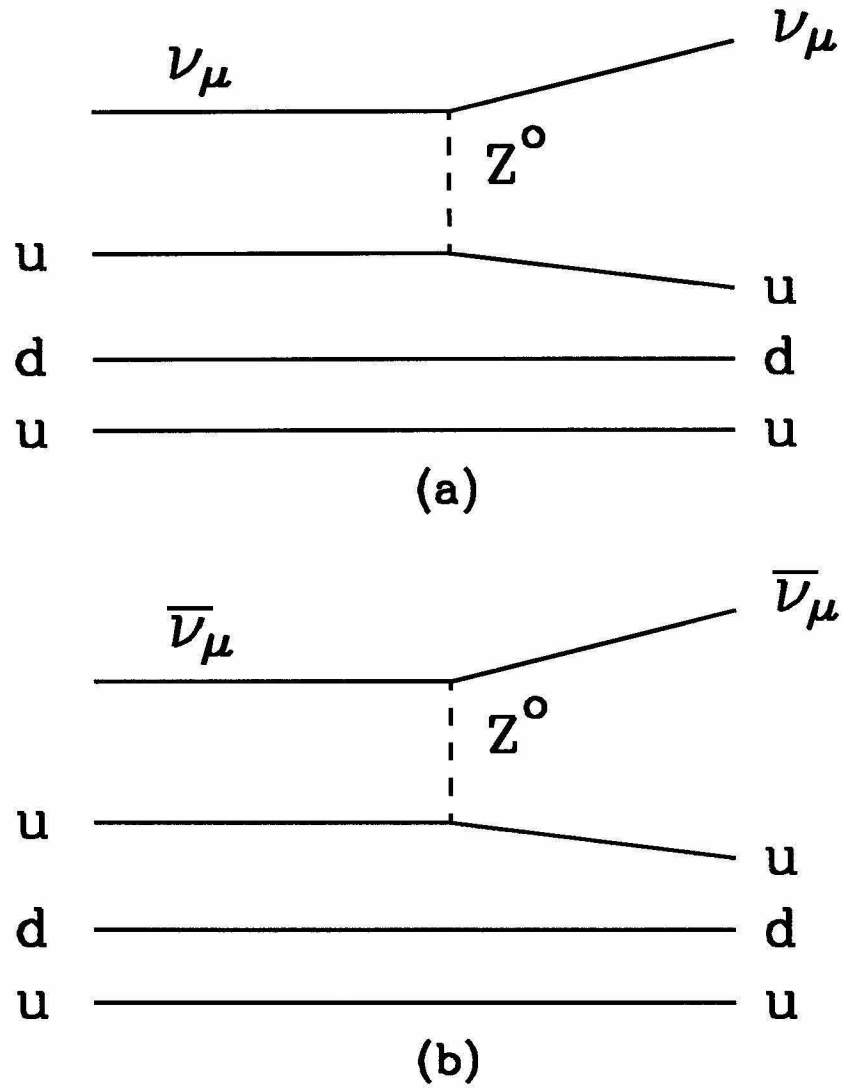

Figure 2.2: Quark diagrams of NC interactions

of finding ν thus becomes complicated. The advantage in our experiment is that there is only one projectile collision per event, so the proton excess may entirely represent the cascade process. For the following reason only slow particles can undergo such rescattering. Hadrons are produced on the time scale of 10^{-23}sec, corresponding to the order of a fermi. Relativistic hadrons see the nucleus as a Lorentz-contracted disk, the size of the contraction controlled by the factor γ. Thus the fast hadrons are produced outside of the nucleus and do not get a chance to reinteract.

In hadron-nucleus experiments the model of Andersson, Otterlund and Stenlund[15, 16] is often used to determine the number of projectile collisions, ρ. The model uses the gray proton distribution with the assumption that "each encounter in the nucleus corresponds to the same distribution of protons, independent of the projectile, and that the different encounters give independent contributions. The only parameter in the model is, for a given nucleus A, $< N_p >^A_{\rho=1}$ (independent of the projectile hadron h):

$$< N_p >^A_{\rho=1} = \frac{< N_p >_{h,A}}{< \nu >_{h,A}}. \tag{2.5}$$

where $< \rho >_{h,A}$ and later $\pi_{h,A}(\rho)$, the probability that the incident hadron h collides ρ times in the nucleus A, are taken from a Glauber calculation with a Woods-Saxon nucleon density distribution"[16]. For our experiment with only one projectile collision the model makes a simple prediction. The fraction of events with N_p protons is expected to be

$$P(N_p) = (1 - x)x^{N_p} \tag{2.6}$$

where

$$x = \frac{< N_p >}{(1 + < N_p >)}. \tag{2.7}$$

Note that the prediction is normalized. We will compare our gray proton distribution with this model as well as with the prediction of the Poisson distribution. If an agreement with the Andersson model is found and if we assume that the entire gray proton excess is due to intranuclear cascade, then we can deduce the average number of secondary collisions in an event.

2.3 Backward Proton Production

In both neutrino-nucleus and hadron-nucleus type experiments the presence of gray protons travelling backwards with respect to the beam direction have been observed. Since nucleons cannot be produced backwards as a result of a collision off of free stationary nucleons, their presence suggests that nuclear effects take place in the scattering process. Many models have been suggested as mechanisms for producing the backward protons, sometimes called cumulative protons. All the models postulate the existence of some organized structure within the nucleus, such as the effective clustering of nucleons. The clusters could be the result of time dependent nuclear density fluctuations, two or three nucleon clusters with greater than average nucleon binding, multiquark bags, or a combination of these. Scattering off of such clusters could produce backward emitted protons.

In Ref.[14] there is an extensive study of backward emitted protons using $p - {}^{20}Ne$ interactions at 300 GeV. It is claimed that although successive rescattering within the nucleus can produce backward protons, it does not explain their abundance or high energy. Such rescattering is claimed to make up only about 30% of the backward proton sample. The process investigated is the absorption of pions in the nucleus by the following reactions:

$$\pi + \text{"}b\text{"} \rightarrow N + N \tag{2.8}$$

$$\pi + \text{"}b\text{"} \rightarrow \Delta + N \tag{2.9}$$

with

$$\Delta \rightarrow N\pi \tag{2.10}$$

where "b" is a nucleon-nucleon system within the nucleus. It is interesting to note that the above processes are another form of rescattering within the nucleus. While in the section regarding intranuclear cascade we only discussed nucleons scattering off of each other in the target nucleus, now we want to see if pions produced in the projectile collision could also go through some form of rescattering. Note that fast pions are formed outside of the nucleus, and only slow ones can reinteract,as explained in the

previous section. In Ref.[14] strong evidence was found in favor of the existence of the above two reactions providing a mechanism for the production of backward protons. We will make a similar analysis and compare our results.

Another method of testing for short range correlations within the nucleus is proposed by Frankfurt and Strikman [11], and investigated experimentally in Ref.[7, 6]. It is assumed that in the nucleus a clustering of two nucleons exists with equal and opposite momenta, thus forming a deuteron-like object. It is thought that when the neutrino scatters off of the nucleon with its momentum vector pointed forward, the other nucleon is liberated with backward momentum. In the process described we label the forward oriented proton the target proton and the backward oriented proton the spectator proton. Note that now we are no longer considering a rescattering mechanism for backward proton production, but the neutrino directly hitting a nuclear cluster. We will look for evidence of such a mechanism by studying possible correlations between the muon and the spectator (or backward) proton.

To test for correlations between the spectator proton and the muon we use $v = xy$, where x and y are the Bjorken scaling variables. We define v_{true} as v for an interaction with a moving target and v_{meas} as v for an interaction with a stationary target.

$$v_{meas} = v_{true}(2-\alpha) \tag{2.11}$$

$$\alpha \equiv \frac{(E_p - p_l)_s}{m} \tag{2.12}$$

where E_p, m and p_l are the spectator or backward proton energy, mass and longitudinal momentum with respect to the neutrino direction[7]. The above relation is derived using the basic assumption that $E - p_l$ of the two-nucleon system is conserved. The target and spectator protons have some initial value $E - p_l$ whose sum is constrained to be twice the nucleon mass[6]:

$$2m = (E - p_l)_s + (E - p_l)_{tar}. \tag{2.13}$$

With the above definition of α we can write

$$\frac{(E - p_l)_{tar}}{m} = 2 - \alpha. \tag{2.14}$$

For a neutrino interacting with a moving target the scaling variable is

$$v_{true} = \frac{Q^2}{2p_{tar} \cdot p_\nu} \tag{2.15}$$

$$= \frac{Q^2}{2(E_{tar}E_\nu - p_{l,tar}E_\nu)} \tag{2.16}$$

$$= \frac{Q^2}{2E_\nu(E - p_l)_{tar}} \tag{2.17}$$

$$= \frac{Q^2}{2E_\nu m(2-\alpha)} \tag{2.18}$$

The Bjorken scaling variables x, y and their product v for a stationary target are:

$$x = \frac{Q^2}{2m\nu} \tag{2.19}$$

$$y = \frac{\nu}{E_\nu} \tag{2.20}$$

$$v = xy = \frac{Q^2}{2mE_\nu} \tag{2.21}$$

For an interaction with a stationary target,

$$v_{meas} = \frac{Q^2}{2E_{tar}E_\nu} \tag{2.22}$$

$$= \frac{Q^2}{2mE_\nu} \tag{2.23}$$

$$= v_{true}(2-\alpha). \tag{2.24}$$

$v_{meas} = Q^2/2mE_\nu$ can also be written in terms of muon variables:

$$Q^2 = (\vec{p}_\nu - \vec{p}_\mu)^2 - (E_\nu - E_\mu)^2 \tag{2.25}$$

$$= p_\nu^2 + p_\mu^2 - 2p_\nu p_{l,\mu} - E_\nu^2 - E_\mu^2 + 2E_\nu E_\mu \tag{2.26}$$

$$= 2E_\nu E_\mu - 2p_\nu p_\mu \tag{2.27}$$

$$= 2E_\nu(E - p_l)_\mu \tag{2.28}$$

Replacing Q^2 in v_{meas} with the equation above,

$$v_{meas} = v_\mu = \frac{(E - p_l)_\mu}{m}. \tag{2.29}$$

α is greater than one for backward protons, because p_l is negative. For events with backward protons $< v_{meas} >$ or $< v_\mu >_{Bp}$, is expected to decrease linearly with increasing α[6]. We will examine the normalized plots:

$$< v_N > = \frac{< v_\mu >_{Bp}}{< v_\mu >} \tag{2.30}$$

where $< v_\mu >$ is the average of v_μ over the whole charged current sample.

It has been shown in Refs.[6, 7, 4] that the normalized invariant differential cross section for backward particles can be parametrized with an exponential:

$$\frac{1}{N_{ev}} \frac{E}{p} \frac{dN}{dp^2} = C \exp(-B(\theta)p^2) \tag{2.31}$$

where E and p are the energy and momentum of the backward particle in the laboratory frame, and θ is the angle between the particle and the beam direction. Hadron experiments have found that the slope $B(\theta)$ does not depend on the energy of the beam particle or the mass number of the target, and C depends on it only weakly[7]. Ref.[6] also showed that B is independent of the type of backward particle, and that it is consistent with values found in an experiment with Deuterium target. The latter result may be an indication that scattering off of two-nucleon systems similar to the deuteron takes place.

Chapter 3

Experimental Description and Apparatus

3.1 Introduction

Data acquisition for the E632 experiment was performed at the Fermi National Accelerator Laboratory utilizing the Tevatron accelerator. Two separate data runs were made in the Neutrino Beamline, one in 1985 and another in 1987-1988. The 15 ft. Bubble Chamber, filled with heavy Ne-H_2 mix, was used for event detection. The External Muon Identifier (EMI) and Internal Picket Fence (IPF) were used for muon detection.

3.2 Beamline

Figure 3.1 shows the layout of the beamline at Fermilab(not to scale). The booster injects protons with energy of 8 GeV into the main ring, which then accelerates them to 150 GeV. From there they are transferred to the Tevatron which accelerates them to 800 GeV. The duration of each accelerator cycle was approximately 60 seconds, during which three spills of protons were dumped into the beamline. Each spill lasted $2-3$ msec and followed each other approximately 10 seconds apart, each containing about $1-2\times10^{12}$ protons.

The proton beam was directed to collide with a 30 cm^3 Beryllium Oxide target, producing secondary particles of pions and kaons. The charged hadrons were focussed by a Quadrupole Triplet Magnet Train, tuned to 300 GeV/c. Hadrons with less than the tuned momentum diverged. The tuned hadron beam was then allowed to enter a 500 m vacuum pipe, where the hadrons decayed to mostly neutrinos and muons by the following decay modes:

$$\pi^+(\pi^-) \longrightarrow \mu^+(\mu^-) + \nu_\mu(\bar{\nu_\mu}) \;\; (B.R.\ 100\%) \tag{3.1}$$

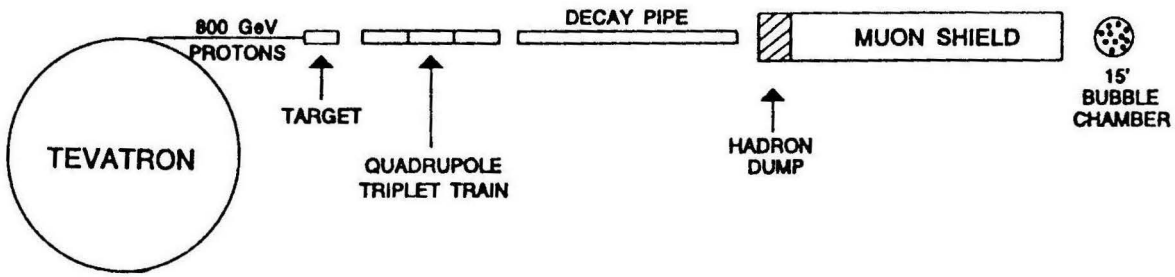

Figure 3.1: Layout of the beamline at Fermilab(not to scale)

$$K^+(K^-) \longrightarrow \mu^+(\mu^-) + \nu_\mu(\bar{\nu}_\mu) \ \ (B.R.\ 63.5\%) \tag{3.2}$$

Approximately 3% of the neutrinos were $\nu_e(\bar{\nu}_e)$, produced by three body decays of K_L^0 and $K^{+/-}$:

$$K^+(K^-) \longrightarrow \pi^0 + e^+(e^-) + \nu_e(\bar{\nu}_e) \ \ (B.R.\ 4.8\%) \tag{3.3}$$

$$K_L^0 \longrightarrow \pi^+(\pi^-) + e^-(e^+) + \nu_e(\bar{\nu}_e) \ \ (B.R.\ 38.7\%) \tag{3.4}$$

In order to produce a neutrino beam as pure as possible, extensive shielding was needed to filter out the secondary hadrons and muons. At the end of the decay pipe an iron dump was used to absorb the hadrons, but most muons continued. In order to stop the muons, a shield of one km length, made of earth and steel, was constructed. The neutrino beam then entered the 15 ft. Bubble Chamber, where neutrino interactions could be recorded and studied.

The beam composition was $\nu : \bar{\nu} = 5 : 2$, the average $\nu(\bar{\nu})$ energy was 80 GeV (70 GeV). Since the neutrino cross section increases linearly with energy, the average charged current $\nu(\bar{\nu})$ event energy was 150 GeV (110 GeV). The primary proton beam intensity was monitored during the run by the Secondary Emission Monitor (SEM) and a toroid upstream of the BeO target.

3.3 15 ft. Bubble Chamber

Figure 3.2 shows the sideways view of the Bubble Chamber. The Bubble Chamber was filled with a heavy Ne-H_2 mix, with an average Neon mole percent of 75% in the 1985 run and 63% in the 1987 run. The density of the liquid was 0.71 g/cm^3 in the 1985 run and 0.54 g/cm^3 in the 1987 run. The radiation length in the 1985 and 1987 runs was 41.5 cm and 55.0 cm. The large radius of the Bubble Chamber, 180 cm, resulted in a high photon conversion rate of approximately 90%[17]. The heavy mixture also gives the advantage of a shorter interaction length, resulting in most hadrons interacting inside the chamber, thus reducing the background in muon detection. The interaction length in the 1985 and 1987 runs was 153 cm and 192 cm.

The function of the Bubble Chamber was to make the neutrino event vertices and the paths of their secondary charged particles visible, so that they can be photographed

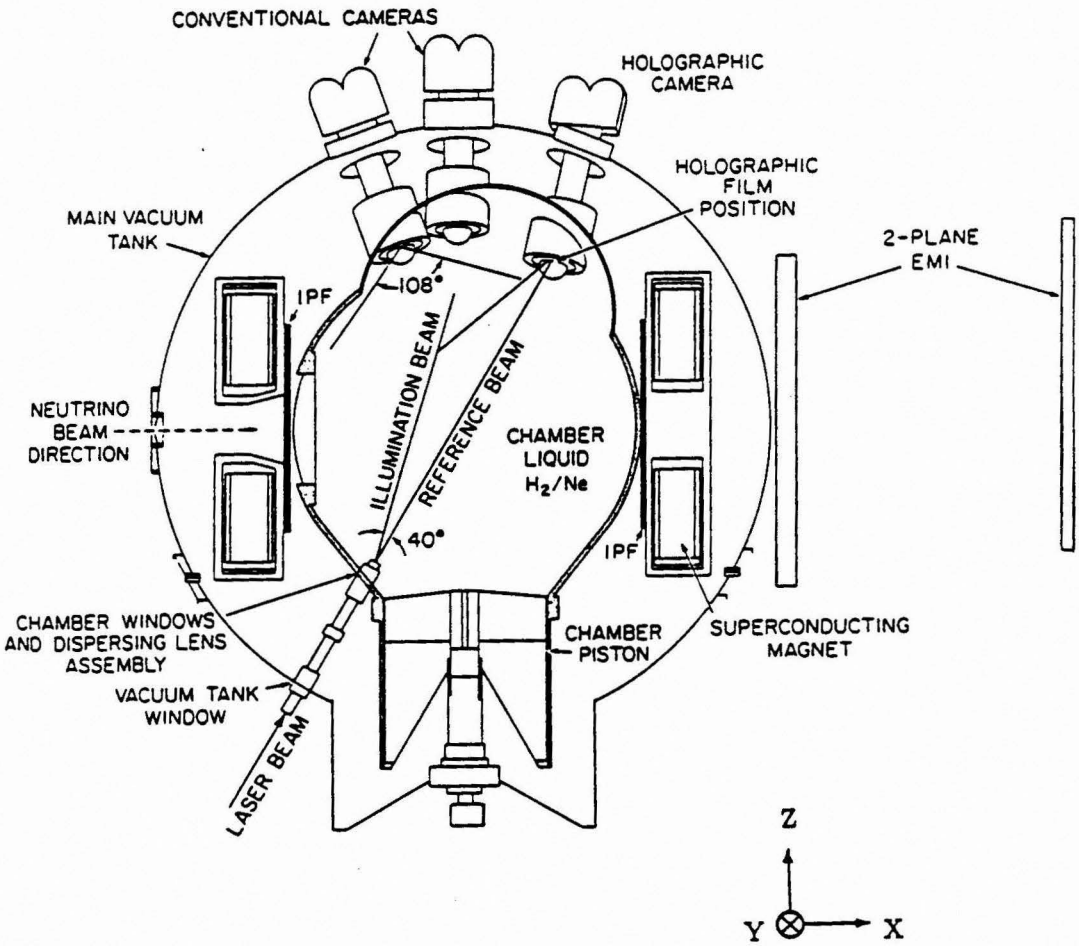

Figure 3.2: Side view of the 15 ft. Bubble Chamber

and studied. The chamber operated at a liquid temperature of 30°K and 3 atmospheres of pressure. The liquid was superheated by lowering the piston at the bottom of the chamber 50 msec before the beam arrival. Boiling of the superheated liquid starts with the formation of small bubbles around ions left behind by charged particles traversing the liquid. The bubbles were allowed to grow to a specific size, the chamber was photographed, and recompressed. The expansion/recompression cycle lasted approximately 100 msec.

The chamber was surrounded by a superconducting magnet, generating a nearly uniform 3 Tesla magnetic field inside the chamber along the z (vertical) axis. The magnetic field deflects charged particles in the x - y plane (horizontal plane). The momenta of the particles can then be determined by measuring the radius of curvature on the photographs.

For taking the photographs, 6 camera ports were fixed on top of the Bubble Chamber. Four cameras (three in 1985) had conventional optics with 400-500 μm resolution, one camera had high resolution conventional optics with 150-200 μm resolution and one other camera was used to take holograms with approximately 100 μm resolution optics. Since there were three separate photographing techniques with different resolutions, each one requiring the bubble size to match its own resolution, there were three separate delay times for taking the pictures. For holograms the delay after beam arrival was 1 msec, for high resolution 2 msec, for conventional approximately 12 msec. For taking holograms the chamber was illuminated by a laser beam directed through a dispersing lens from the bottom of the chamber at a location immediately next to the chamber piston. Annular flash tubes located behind each camera window illuminated the chamber for the conventional photographs. The inner walls of the chamber were lined with Scotchlite which has the property of directing a light beam back to its place of origin. Thus on the negatives the Scotchlite provided a dark background. The bubbles appeared white on the film, as they scattered the reflected light. The cameras each had a wide angle lens with 108° field of view, separated from the chamber liquid by fisheye windows. A total visible volume of 28 m^3 was reached with the conventional cameras, approximately 1 m^3 with the high resolution conventional camera and greater

than approximately 3 m^3 with the holographic camera.

3.4 EMI-IPF

Figure 3.3 shows the arrangement of the IPF and the EMI planes with respect to the BC and the coordinates in EMIB. The External Muon Identifier (EMI) and Internal Picket Fence (IPF) were both made up of layers of proportional counters. The IPF's counters surrounded the chamber and the EMI was located further downstream of the chamber. The counters discharged anytime a charged particle passed through them, and this information was combined with the information gathered from the Bubble Chamber pictures for use in the analysis. The upstream section of the IPF was used to veto events caused by interactions upstream of the Bubble Chamber. The downstream section of the IPF was used to help determine the event time for Neutral Current (NC) and Charged Current (CC) events. The IPF was used extensively in the NC analysis[18]. The EMI was used to identify muons. Muons interact less readily than hadrons, so installing absorbing materials between the different planes of the EMI made it possible to positively identify particles which got through to the final plane as muons.

The IPF was located in the outer vacuum vessel of the Bubble Chamber. It had two sections: IPFA was located upstream, IPFB downstream of the vessel. Together, they almost completely surrounded the chamber, covering 290° in azimuth and having a surface area of 23.2 m^2. A total of 96 cans each contained 24 vertical cylindrical proportional tubes. The tubes had an inner diameter of 7 mm, a wall thickness of 0.5 mm and length of 220 cm. A 50 μm thick gold plated tungsten wire in the middle of each tube functioned as the anode, and was at approximately 1750V high voltage. The tubes were filled with an 80-20% mixture of Ar-CO_2.

The EMI consisted of three vertical planes (EMIA, EMIB, EMIC). EMIB had three staggered double layers of proportional tubes, one horizontal, one vertical and one diagonal at 36.5^o with respect to the vertical direction. The tubes were 220 cm long and 2.5 cm $\times$ 2.5 cm wide. As in the IPF, the anode was a 50 μm gold plated tungsten wire, but at 2400V, and the gas inside the tube was an 80-20% mixture of Ar-CO_2. EMIA

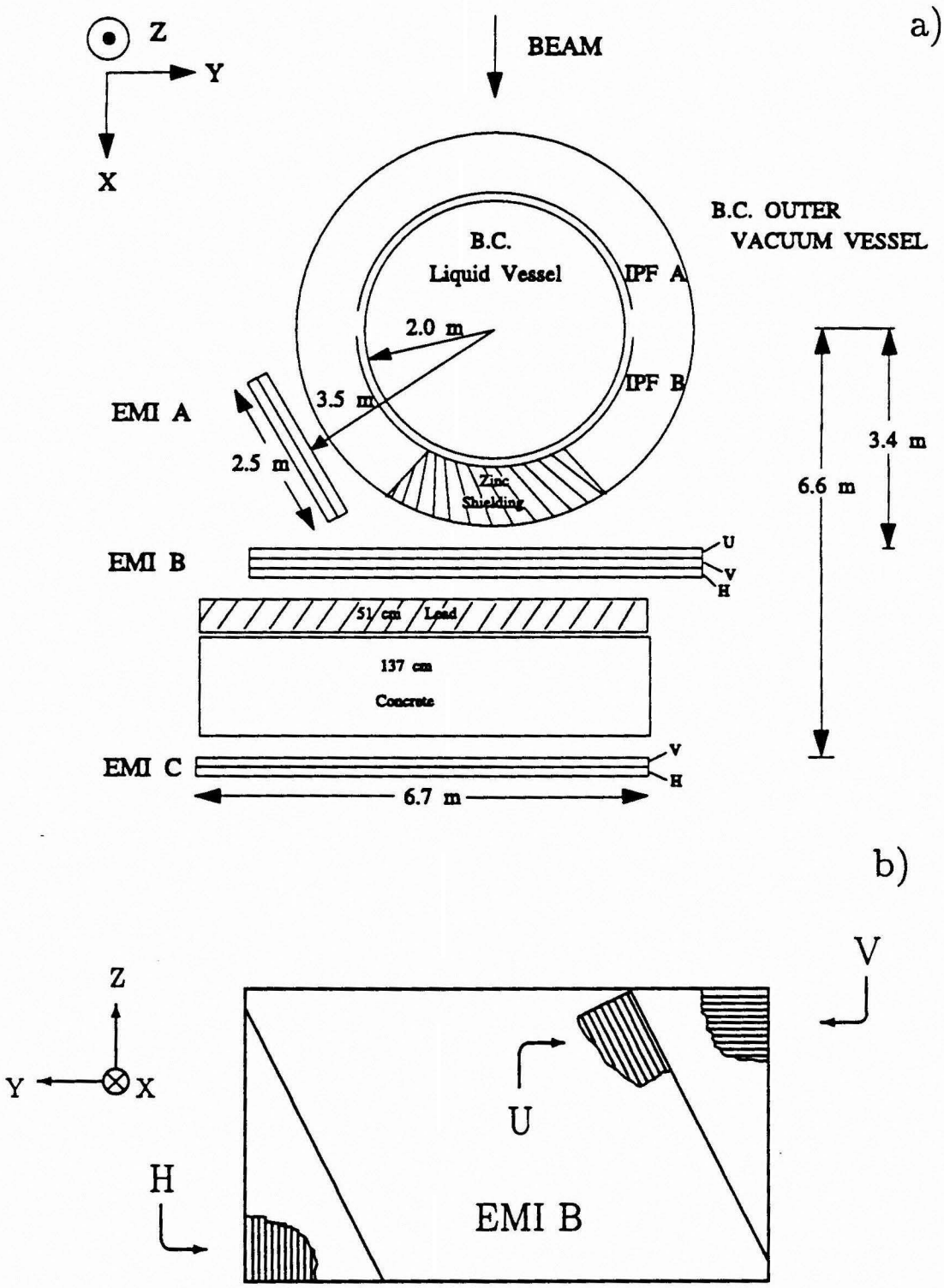

Figure 3.3: a) Top view of the IPF and the EMI planes. b) The arrangement of the three coordinates of the EMIB.

and EMIC were also made up of double layers of proportional tubes, but without the diagonal layers. EMIA stood at the downstream right side of the chamber, having the purpose of catching lower energy muons, which were bent enough by the Bubble Chamber's magnetic field not to reach EMIB or EMIC. EMIC was downstream of EMIB, both perpendicular to the beam. There were walls of concrete and lead shielding between the Bubble Chamber and EMIB and between EMIB and EMIC. So hadrons leaving the chamber would travel 10 hadronic interaction lengths to reach EMIC, making EMIC an effective muon detector.

The signals from the EMI/IPF tubes were multiplexed together; in the case of the EMI, 15 tubes and in the case of the IPF, 12 tubes were multiplexed onto a single cable. A 16 MHz clock arranged the output into 1 μsec time slots. The EMI/IPF gathered data for 4 msec starting at each beam arrival. The data was demultiplexed at the CAMAC crate in the EMI control room. A PDP11/45 computer was interfaced to the CAMAC crate and was used to write the EMI/IPF data directly to magnetic tape. The roll and frame numbers as well as neutrino beamline data were also recorded for each picture taken. The online data acquisition was done by a program called RTMULTI, written at Fermilab. In addition to writing the data to tape, it was also used to test the hardware and to do some data checking with the use of some histograms and scatterplots.

Chapter 4

Data Collection and Reduction

4.1 Scanning

During the course of the E632 experiment approximately 330000 pictures were taken, corresponding to 5.5×10^{19} protons on target. The pictures were taken on 70mm film, each roll containing approximately 1000-2000 pictures. These rolls were distributed among the participating labs. Each lab had trained technicians who searched the film for neutrino events and measured them. The scanning and measuring was done on large projection machines which had a film to table magnification in the range of 30 to 70 times. For each picture three conventional views were completely looked over. Depending on the neutrino flux one neutrino event candidate was found on the average of once in every 5 to 10 frames. When an event was found, it had to meet the following criteria to be recorded: 1.) The vertex of the event had to be visible in all three views (it could not be measured without a recorded vertex). 2.) It could not be associated to another event which took place in the chamber, on the wall or outside the chamber. 3.) It had to have at least 5 GeV/c momentum, which could be measured roughly with a momentum template. 4.) The vertex of the event could not be located on the wall of the chamber. 5.) The event had to have a potential length to the back wall of at least 35 cm. The vertices were reconstructed by a computer program, so their exact location in the chamber was determined. A fiducial volume was imposed, so that events close to the walls, too high or low in the chamber, or with short potential length were not passed on to the measuring stage. The rejected events would have yielded a poor measurement either due to blurriness or because short high energy tracks with little curvature would yield a poor momentum measurement.

A complete scan was done twice on most of the distributed rolls in order to calculate

a scanning efficiency. The overall scanning efficiency was 98%.

4.2 Measuring

After the fiducial volume cut was made, the events were passed on to the measuring stage. Not all events found could be measured at all labs, however, due to some shortage of manpower. The name minimum bias sample usually refers to a sample of events for which no physics cuts were made besides the conditions which the events had to meet at the scanning table. So for our minimum bias sample all events were measured on a total of 75000 frames. Selected events were measured on the rest of the film for special topics.

The events were measured with the help of an online program; as the measurer entered the points along the tracks of an event, the coordinates from two electronic encoders were directly sent to a file to be later processed by a geometry reconstruction program. The measurer was instructed to measure all charged tracks, gammas (photon conversions) and V^0's (strange particle decays) and neutron stars (neutron interactions) pointing to the primary vertex. A minimum of $5-10$ points per view were recorded for every track, and a code was entered after the concluding point depending on whether that track was leaving, stopping, interacting, decaying or an electron type track. The event had to be measured in all three conventional views, although if a track was completely obscured in a view, then a two-view measurement was acceptable. In order to be able to reconstruct the events, some previously surveyed fiducial marks located on the chamber had to be measured. The marks chosen varied from lab to lab; Rutgers measured three fiducial marks on the 1985 film and six on the 1987 film.

4.3 Scanning/Measuring Difficulties

In the course of the data acquisition several difficulties arose. The chamber conditions during the run were not always ideal. In the 1985 run the delay time for the conventional cameras was set for 1 msec instead of 12 msec for a large fraction of the rolls (80% of the frames). Thus the bubbles did not grow to a proper size and the tracks of the events

tended to be faint and almost invisible in the lower parts of the chamber. Not only was it difficult to measure the events, but the scanning efficiency suffered, especially for lower topology events. In the 1987 run the bubble chamber was filled using a filter with larger mesh spacing than was required and about 1 cm^3 water entered the chamber. This water deposited as ice on the lower third of the chamber wall's bottom, rendering the Scotchlite ineffective. The background became light instead of dark, so it became difficult to find the light tracks. The early phases of the deposit were still manageable, but the problem grew progressively worse until the chamber was emptied, scrubbed out and refilled. Approximately 30% of the frames were affected.

Due to the high energy of this experiment, some of the higher energy events looked undecipherable on the scanning table and could not be measured fully. Measuring an event became difficult if it had a high charged track multiplicity; some events also exhibited a jet-like appearance, with several very high energy forward directed charged tracks, sometimes compounded with the presence of a gamma shower in the jet. Such events were examined very carefully and measured as fully as possible, with special attention given to finding leaving tracks (for muon identification) and V^0's. Most labs had a partial measuring rate of around 5% in the 1985 film and $1-2\%$ in the 1987 film.

4.4 Data Reduction

The data entered by the measurer using the online program was sent through a chain of programs in order to prepare it for analysis. First the events were reconstructed using a geometry program developed at CERN. It reconstructed the charged tracks with several mass fits depending on the track type, and did kinematic fitting of the neutral gammas and V^0's to the primary and/or secondary vertices. The best fit was selected for the neutrals; non-pointing neutrals and neutrals pointing to secondary vertices were disregarded in the energy calculation of the primary event. Some labs did quality checks of their measurements and remeasured parts of some events. Using a package of programs, part of the original measurement of an event could be deleted and the remeasurement merged in. At Rutgers all events were rechecked at least once. The output of the CERN geometry had a standard format, so this information could

be exchanged among different labs.

A second set of programs was used to flag muons. A data tape from the original EMI run containing all the hits was used, and a program extrapolated the leaving tracks from the given event to try to match them with the hits. A muon was identified when there was a good match in both EMIC planes and in two of the three EMIB planes in the same time slot. If an event was found to have more than one muon, then the one with the higher energy was kept as the true muon. The output of this set of programs was also in standard format, and it was this type of data most frequently exchanged among labs. For extensive detail on the chain of programs used, see Ref.[19].

Studies of the EMI efficiency showed that the geometrical acceptance is about 99% for muons with $p > 10$ GeV/c, and it is $(73.7 \pm 2.3)\%$ for μ^- at $5-10$ GeV/c. A Neutral Current event is sometimes misidentified as a Charged Current event when a charged hadron leaves the chamber and is not stopped by the absorber,thereby producing hits in EMIB and EMIC just like a muon would. For $p_\mu > 5$ GeV/c the contamination is estimated to be $0.9 \pm 0.3\%$, see Ref. [17].

A program was written at Rutgers to condense the final data from all labs into a simplified data structure (DST) to be used locally for analysis. Some editing of this data was possible, including the deletion, addition and flagging of primary charged tracks. The flags were used only in the proton analysis, which is the topic of this thesis.

4.5 Proton Flagging

Protons can be identified in the events, because unlike other particles which interact or decay, they stop and get absorbed by nuclei in the liquid. Their momentum can be ascertained from a well known momentum-range table which the geometry program utilizes. The program also cross-checks against the track's momentum from curvature. However, in the Neon liquid there appeared to be significant multiple scattering of slow tracks, and an effort was made at Rutgers to find not only the stopping protons, but the scattering ones as well. The scanners were instructed to look up all positive tracks which had momenta below 1.5 GeV/c. 25 rolls from various labs were rechecked,

Table 4.1: Number of gray protons in each flag category

Event type	0	1	2	3	4	5
CC	1530	44	210	88	38	32
All Events	3923	117	431	194	82	53

corresponding to 50% of the minimum bias sample.

Positive tracks which kinked and stopped were considered as protons as long as the total length of the track indicated a momentum from range consistent with the momentum found by the geometry program, and if no neutral particles pointed to the kink in the track.

Flags were assigned depending on the proton's behavior as follows: 0 - Stopping proton. 1 - Stopping proton, but found in the course of rechecking. 2 - A kink present near the end of the track, with a length after the kink less than what is consistent with the Fermi momentum of 350 MeV/c. 3 - A kink along the track with a length after the kink longer than described in category 2. 4 - A track which was originally thought to be a proton but was reassigned as a pion during the proton checking process. 5 - A long stopping track for which the geometry program does not yield a momentum from range, but a momentum from curvature - a problem thought to be with the tolerances present in the geometry program, not with the measuring or with the track.

Tracks with flags 0,1,2,3 and 5 were used in the analysis as protons. The number of gray protons in each used flag category is listed in Table 4.1 for CC events and for all events.

Chapter 5

Data Sample Selection

5.1 Selection of Charged Current and Neutral Current events

The muon in a CC event was required to have a 4 plane match in the EMI (see the discussion of EMI planes in the chapter on apparatus), and a minimum energy of 5 GeV. There is a minimum total energy of 5 GeV required for events in the Neutral Current sample. This cut is imposed in order to cut out most of the neutron star background. In some of the analysis we will use CC events only, in others, all events. The list of events in each category is given in Table 5.1.

5.2 Energy Correction for Charged Current Events

Measuring the charged tracks and associated neutral particles of an event yielded the total energy of the event, however, this energy had to be corrected to compensate for neutral particles which escaped the chamber. The Bonn method, based partly on balancing the transverse momentum, was selected. The corrected neutrino energy is calculated using:

$$E_\nu = P_\mu^L + \Sigma P_h^L \left[1 + \frac{\left| \vec{P}_\mu^T + \Sigma \vec{P}_h^T \right|}{\Sigma \left| \vec{P}_h^T \right|} \right] \tag{5.1}$$

Table 5.1: Minimum bias event sample

CC	3898
$C\bar{C}$	738
NC	3853
Total	8489

The energy spectrum using this correction is in good agreement with a Monte Carlo calculation using the beam profile[19]. The average correction to the visible energy is 9%. As mentioned in section 4.3 some difficult events were measured incompletely, and the Bonn correction above undercorrected. In some cases such high energy events were not measured at all or only the muon was measured, and the Bonn correction was not useful. Although we expect an average CC event energy to be 150 GeV, we find the corrected event energy to be 136 ± 2 GeV. We expect approximately half of the event energy to be that of the muon. We see that a large part of the energy loss is due to missing hadrons, because the average Bonn corrected hadronic energy is 58 ± 2 GeV.

5.3 Separation of Black and Gray Protons

For the physics analysis we want to select a sample of protons which were produced during the deep inelastic interaction of the neutrino with the Neon nucleus. These are sometimes called gray protons. In addition to these protons there are other very low energy protons which are thought to be generated subsequent to the interaction in what is commonly called the evaporation of the Neon nucleus. These are sometimes called black protons and we want to eliminate them from the sample. They may have a momentum of up to 350 MeV/c which is the maximum Fermi momentum for protons inside the nucleus. One way to eliminate the black protons is to discard all protons with less than the maximum Fermi momentum. However; this would eliminate all gray protons with less than 350 MeV/c momentum. An empirical way to make this separation is to plot the cosine of the space angle β with respect to the neutrino beam for both black and gray protons

$$\cos(\beta) = \frac{p_x}{p} \tag{5.2}$$

with

$$p_x = p \cos\lambda \cos\phi, \tag{5.3}$$

where λ and ϕ are the dip and azimuthal angles with respect to the neutrino direction (see Figure 5.1 for the coordinate system including the angles in the Bubble Chamber).

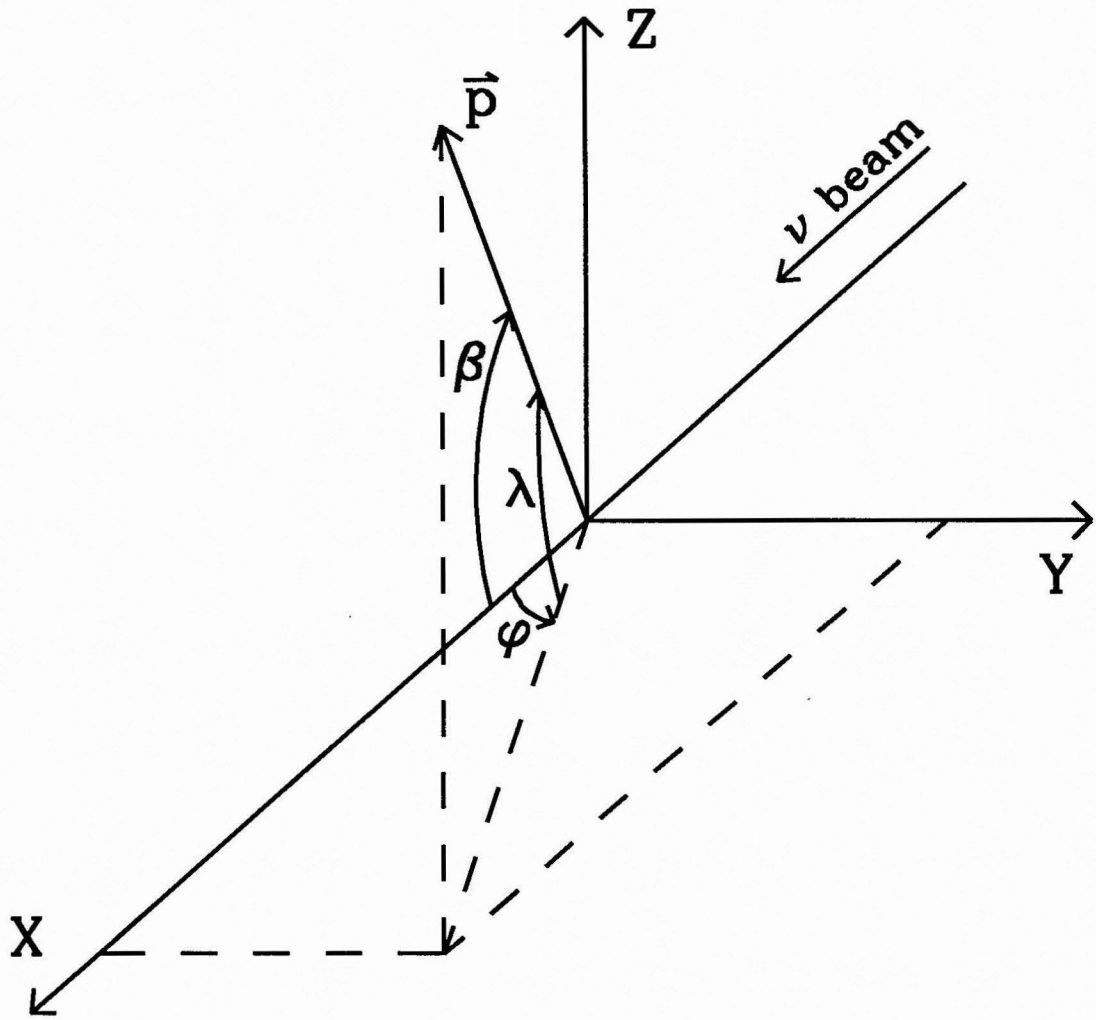

Figure 5.1: Bubble Chamber coordinate system

Table 5.2: Gray proton multiplicity

n_p per event	from CC	from All
0	2574	5520
1	890	1996
2	324	696
3	80	206
4	26	54
5	2	9
6	2	8

The black protons are expected to have an isotropic distribution, since they generally represent the breakup of the nucleus at rest; the gray protons are expected to have an accumulation in the forward direction[20]. We made these plots with various cuts, and settled on 300 MeV/c as the boundary between black and gray protons. The plot for black protons is flat (Figure 5.2), and the plot for gray protons shows a significant rise in the forward direction (Figure 5.3). When we made the plots with a higher cut, then the black proton plot showed an accumulation in the forward region; when we made the plots with a lower cut, then the gray proton plot showed an increase in the backward region.

The momentum distribution of all protons is shown in Figure 5.4. The maximum allowed momentum for a gray proton was taken to be 1.2 GeV/c, because the range of most of these protons would take their endpoints outside of the chamber. The contents of the first bin ($p < 50$ MeV/c) were excluded, because protons having such low momentum could not possibly be identified, and were the result of a failure of the geometry reconstruction program due to the difficulty of measuring such short tracks. The bin contained approximately 80 very low energy protons.

The black and gray proton multiplicity in CC events and in all events is shown in Table 5.2. The total number of gray protons in the CC sample is 1904, and in all events the total is 4315. In CC events the mean number of black protons is 0.39 ± 0.01, and the mean number of gray protons is 0.49 ± 0.01.

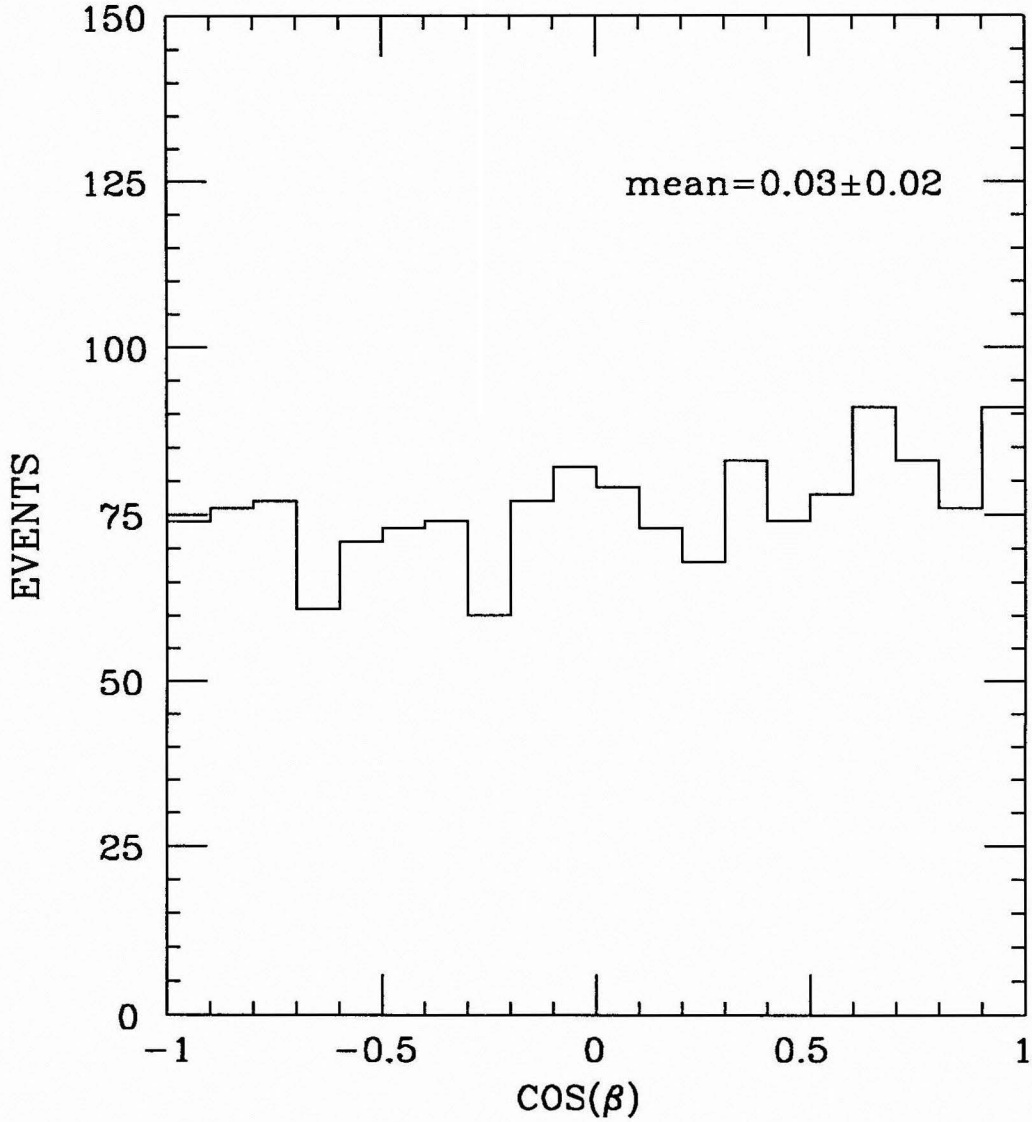

Figure 5.2: $\cos(\beta)$ for protons with $p < 300$ MeV/c

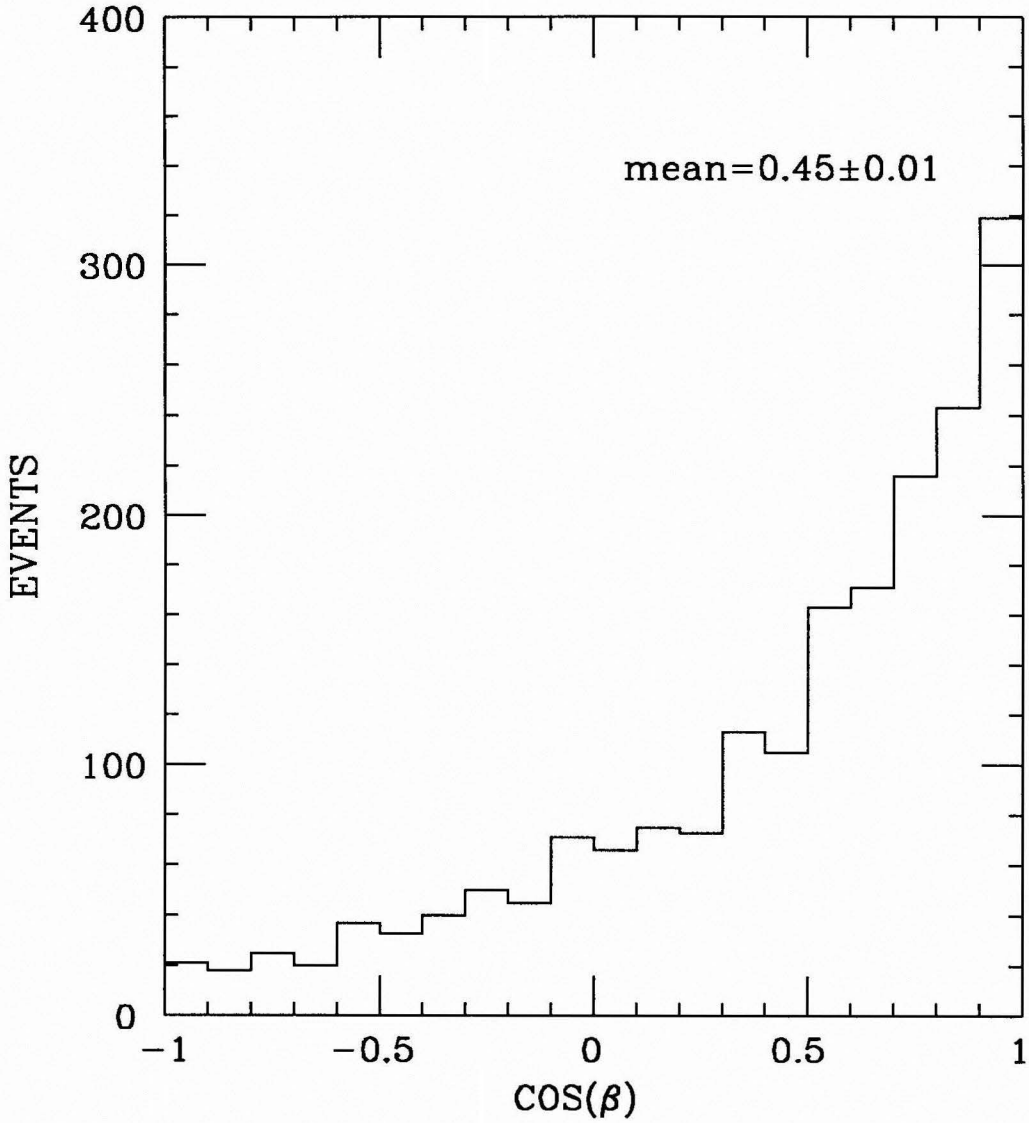

Figure 5.3: $\cos(\beta)$ for protons with $p \geq 300$ MeV/c

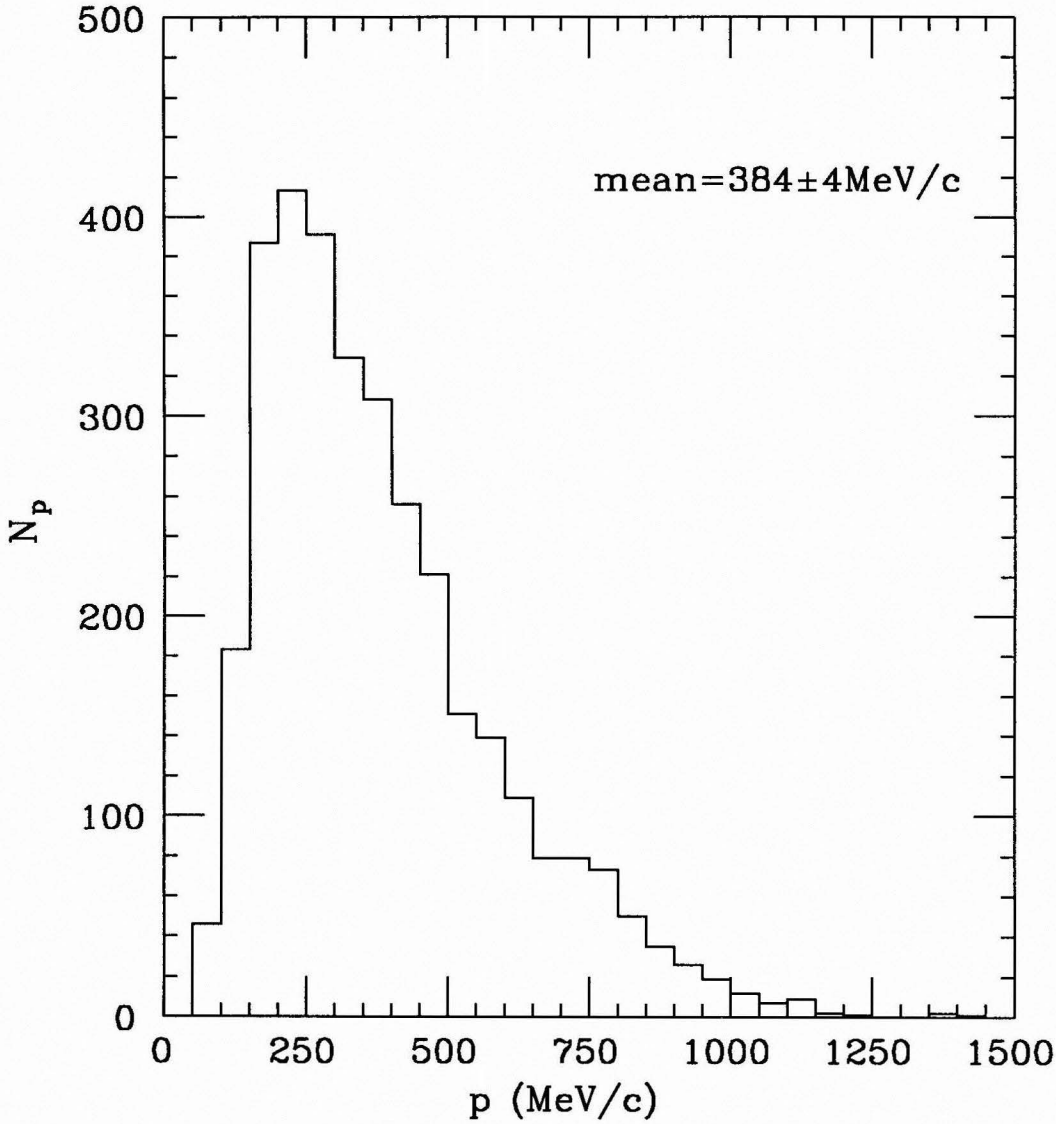

Figure 5.4: Momentum distribution of all protons

Table 5.3: Forward/backward gray proton multiplicity in all events

Forward across Backward down	0	1	2	3	4	5	6	Total
0	5520	1662	455	88	17	3	3	7748
1	334	208	94	24	4	2	0	666
2	33	22	12	1	3	0	0	71
3	2	1	1	0	0	0	0	4
Total	5889	1893	562	113	24	5	3	

5.4 Backward Proton Selection

There is a section in the analysis which deals with primarily backward protons. We define a backward proton as one that is produced at an initial angle of 90° or more with respect to the neutrino direction in the laboratory frame. In other words it is a track with $\cos(\beta) < 0$. The forward versus backward proton multiplicity is shown in table 5.3. The total sample consists of 4315 gray protons, 3495 of which are forward and 820 are backward.

Chapter 6

Physics Results

6.1 Intranuclear Cascade in $\nu_\mu - Ne$ Charged Current Interactions

In this section we look for experimental evidence for secondary collisions in $\nu_\mu - Ne$ charged current interactions. The signal for this is thought to be provided by the number of gray protons in a given event. The distribution of gray protons will be compared with the model of Andersson, Otterlund and Stenlund[15, 16].

6.1.1 Net Charge Excess

Table 6.1 shows the mean number of charged tracks, positive tracks, negative tracks, the mean charge and the mean number of gray protons in CC events. Low energy black protons are excluded from the track multiplicities. We notice that there is a positive net charge which could be an indication that there are secondary collisions taking place. We first want to know what the net charge would be without secondary collisions. Neon has equal numbers of protons and neutrons; however, CC interactions occur about twice as often on neutrons(udd) as on protons(uud), because the W^+ interacts only with the d quark. The experimental average neutron to proton cross section ratio is 1.96 ± 0.07[8]. This value is very close to the theoretical ratio which can be calculated

Table 6.1: Mean multiplicities

$< n_{ch} >$	7.26 ± 0.05
$< n_+ >$	4.00 ± 0.03
$< n_- >$	3.26 ± 0.03
$< n_+ - n_- >$	0.73 ± 0.02
$< n_p >$	0.49 ± 0.01

using the values of the quark structure functions calculated by Field and Feynman, [21], (See Appendix A). A $\nu - n$ interaction would produce an event with net charge of zero, a $\nu - p$ interaction an event with net charge of one, so the mean net charge without secondary collisions is expected to be

$$< Q >_{no\ cascade} = \frac{\sigma_{\nu-p} < Q_{\nu-p} > + \sigma_{\nu-n} < Q_{\nu-n} >}{\sigma_{\nu-p} + \sigma_{\nu-n}} \tag{6.1}$$

$$= \frac{< Q_{\nu-p} > + (\sigma_{\nu-n}/\sigma_{\nu-p}) < Q_{\nu-n} >}{1 + \sigma_{\nu-n}/\sigma_{\nu-p}} \tag{6.2}$$

$$= \frac{1+0}{1+1.96} \tag{6.3}$$

$$= 0.34 \pm 0.01. \tag{6.4}$$

The charge excess is

$$< Q >_{observed} - < Q >_{no\ cascade} = 0.39 \pm 0.02. \tag{6.5}$$

Since there is a charge excess, we have confirmed that there is some rescattering taking place. We want to find the composition of this charge excess, and find out if it could be made up of gray protons.

6.1.2 Proton Excess

We seek to show that the charge excess we found is consistent with being made up of gray protons which are produced by intranuclear cascade. To find an excess of protons which could be produced by cascade we first need to find the mean number of protons which would occur even without cascade. We use a subsample of the CC events, where the events have zero net charge. These events should be a reasonably pure sample of $\nu - n$ events without secondary collisions. In these events

$$< n_p >^{(\nu-n)}_{no\ cascade} = 0.19 \pm 0.01. \tag{6.6}$$

We also need to know the mean number of protons from $\nu - p$ collisions. In a $\nu - n$ collision the W^+ interacts with the d quark of the neutron(udd) and produces a u quark. Then the remainding (ud) diquark has to find a u quark from the sea to make a proton. Due to strangeness suppression it finds a u quark approximately 40% of the

time, a d quark 40% and an s quark 20% of the time. So in a $\nu - n$ collision a proton is produced approximately 40% of the time. In a $\nu - p$ collision the remainding diquark is (uu) which combines with a d quark 40% of the time and with a u quark 40% of the time, and since a (uuu) is a $\Delta^{++} \longrightarrow p + \pi^+$, we get a proton a total of 80% of the time. So without cascade, a proton is produced twice as often in $\nu - p$ collisions as in $\nu - n$ collisions.

$$< n_p >^{(\nu-p)}_{no\ cascade} = 0.38 \pm 0.02. \tag{6.7}$$

Using the above measured value for the mean number of gray protons produced in $\nu - n$ events without cascade,

$$< n_p >_{no\ cascade} = \frac{2 < n_p >^{(\nu-n)}_{no\ cascade} + < n_p >^{(\nu-p)}_{no\ cascade}}{3} \tag{6.8}$$

$$= 0.25 \pm 0.02. \tag{6.9}$$

$$< n_p >_{excess} = < n_p >_{observed} - < n_p >_{no\ cascade} \tag{6.10}$$

$$= 0.24 \pm 0.02. \tag{6.11}$$

We do see a net excess of protons. Since we have some losses in the identification of proton tracks during measuring, we need to calculate some correction factors for the proton excess.

6.1.3 Weights for Protons

Protons are identified during the measuring stage only if they stop, or kink and stop in the chamber. They may also interact or leave the chamber, and we have to correct the proton excess for each case.

For the momentum dependent interaction weight we first assumed all interacting tracks to be pions, and found the average interaction length in several momentum bins using a method of maximum likelihood. The interaction length for protons was found in the same momentum bins by comparing the known momentum dependent cross sections with the interaction lengths. The momentum dependent interaction length for the 1985 film is listed in Table 6.2. Since the bubble chamber liquid was less dense in 1987 by a

Table 6.2: Gray proton interaction lenghts in '85 film

Momentum range (GeV/c)	Interaction length (cm)
$p < 0.4$	45
$0.4 < p < 0.5$	75
$0.5 < p < 0.6$	115
$0.6 < p < 0.7$	125
$0.7 < p < 0.8$	120
$p > 0.8$	125

factor of 0.76, the interaction length was simply divided by that factor for protons in the 1987 film. The interaction weight is

$$W_{int.} = e^{p_l/p_{int.l}}, \tag{6.12}$$

and the average over the whole sample was found to be 1.34 ± 0.01, see Figure 6.1.

For finding the weight due to protons which leave the chamber we employed a method of smearing. The endpoint coordinates of each gray proton are known, and we preserve the relative locations of these coordinates to the location of the primary vertex. Then we randomly place the primary vertex of the event inside the chamber while staying inside the fiducial volume. The location of the proton's endpoint is then calculated, and it is found to be either inside or outside of the chamber. The effective radius of the chamber is taken to be 190 cm (see Figure 6.2), and the bottom of the chamber is taken as -140 cm which is the approximate location of the piston. For each proton this technique is employed 50 times. The average weight for leaving protons is found to be 1.06, so the total weight to be used for the interacting and leaving correction is 1.43 ± 0.01.

6.1.4 Results of Intranuclear Cascade Analysis

Using the above weight the corrected gray proton excess is

$$< n_p >_{excess\ corr.} = 0.34 \pm 0.02. \tag{6.13}$$

Comparing with the charge excess of 0.39 ± 0.02, the charge excess resulting from rescattering is consistent with being mostly made up of gray protons.

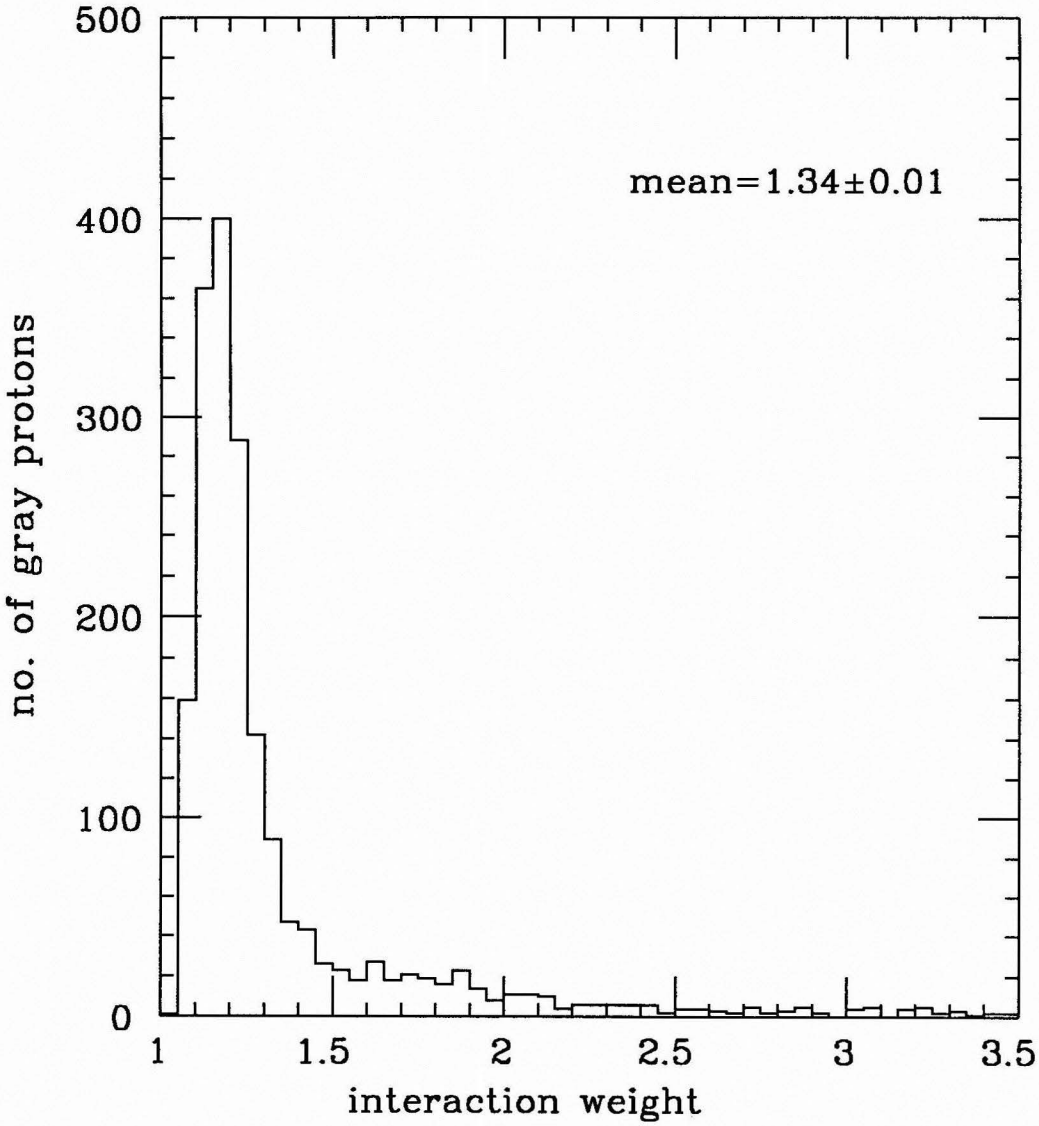

Figure 6.1: Interaction weight for gray protons

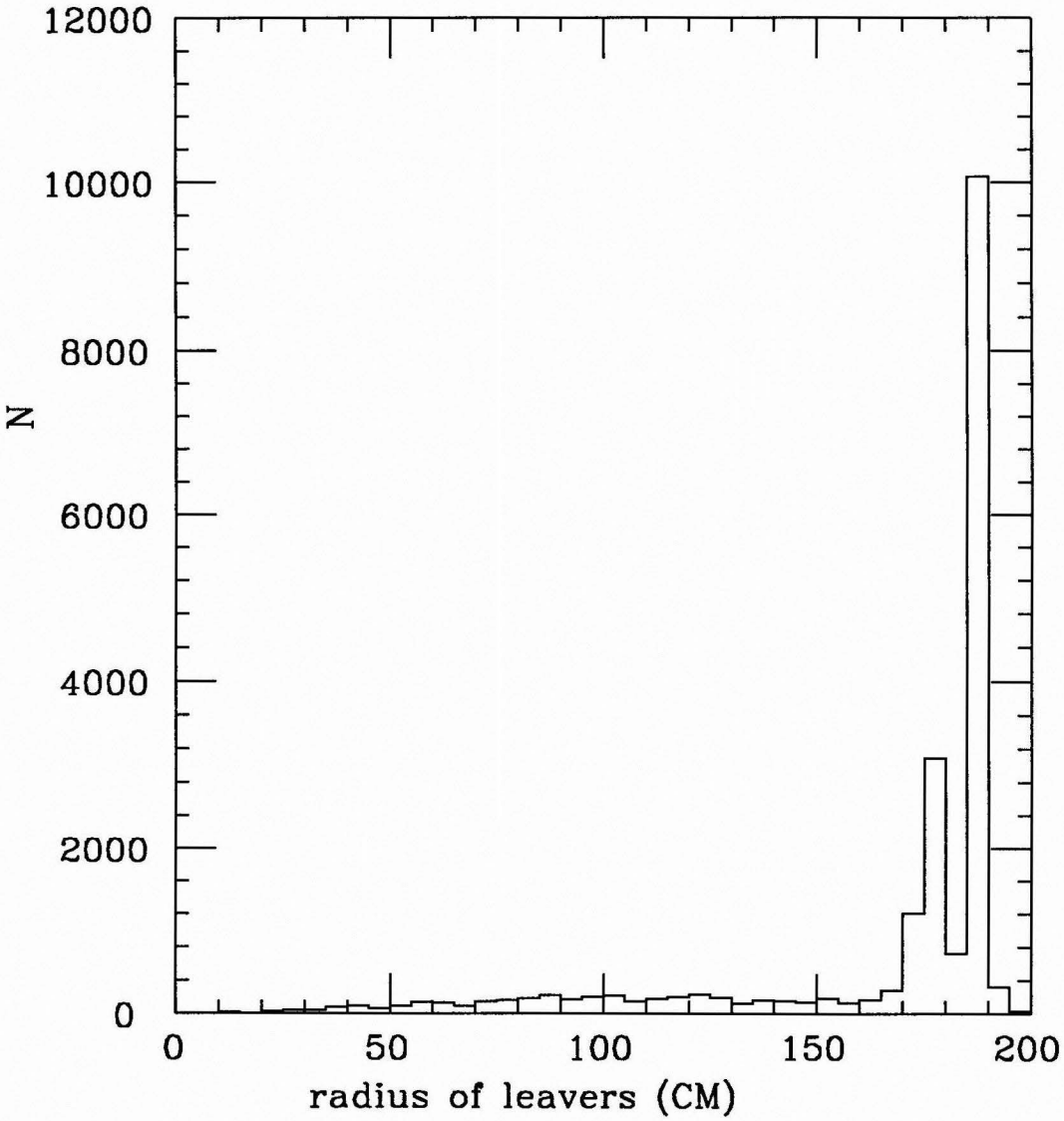

Figure 6.2: Plot of the radius of leaving tracks

To find the average number of secondary collisions we note that a collision off a neutron would not change the net charge of an event, while a collision off a proton would increase it by +1. So the net charge excess is simply half of the number of secondary collisions in an event. The mean number of secondary collisions then is 0.78 ± 0.04.

Figure 6.3 shows the mean charge excess versus the number of gray protons. The plot has a linear rise, and a straight line fit produces a slope of 0.73 ± 0.03. The value of the charge excess versus the number of gray protons averaged over the whole sample is $0.39 \pm 0.02/0.49 \pm 0.01 = 0.80 \pm 0.04$, which is consistent with the slope of the curve. Note that we are plotting against the raw number of gray protons, not the gray proton excess with the above weights applied. Thus even though we claim that most of the net charge comes from gray protons we do not necessarily expect the slope of this curve to be 1. However, we do see a linear rise showing that the net charge rises proportionally with the number of gray protons.

Figure 6.4 shows the fraction of events versus the number of gray protons. The solid line represents the Andersson, Otterlund and Stenlund model for one projectile collision. The model predicts the distribution based only on the average number of gray protons. The dashed line shows the Poisson distribution using the same data points. Both distributions use the average number of gray protons per event as a parameter, so for 7 data points both have 6 degrees of freedom. The χ^2 per degree of freedom is 7.1 for the Andersson model and 23.0 for the Poisson distribution. Although χ^2 for the Andersson model is large, in examining the figure we notice that the majority (5.3) of the χ^2 per degree of freedom is due to one single data point, and in general the data is in good agreement with the model. On the other hand the Poisson distribution does not describe the data.

Table 6.3 shows the average gray proton multiplicity for three ranges of Q^2, the square of the four-momentum transfer to the hadronic system. Table 6.4 shows the same for three ranges of W^2, the effective mass squared of the hadronic system. We see a trend that the gray proton multiplicity decreases when there is a high energy hadronic system present. Although we may not make a direct comparison with results

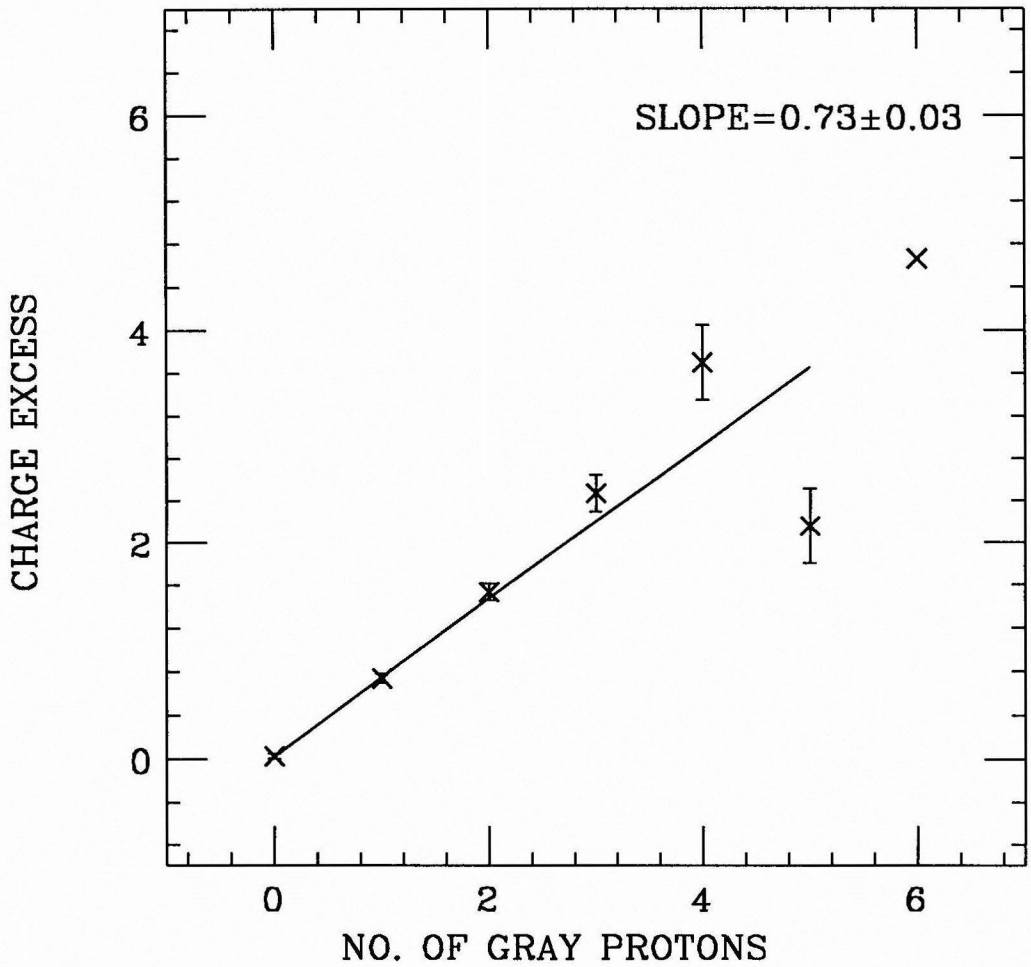

Figure 6.3: Charge excess of an event versus the number of gray protons in the event

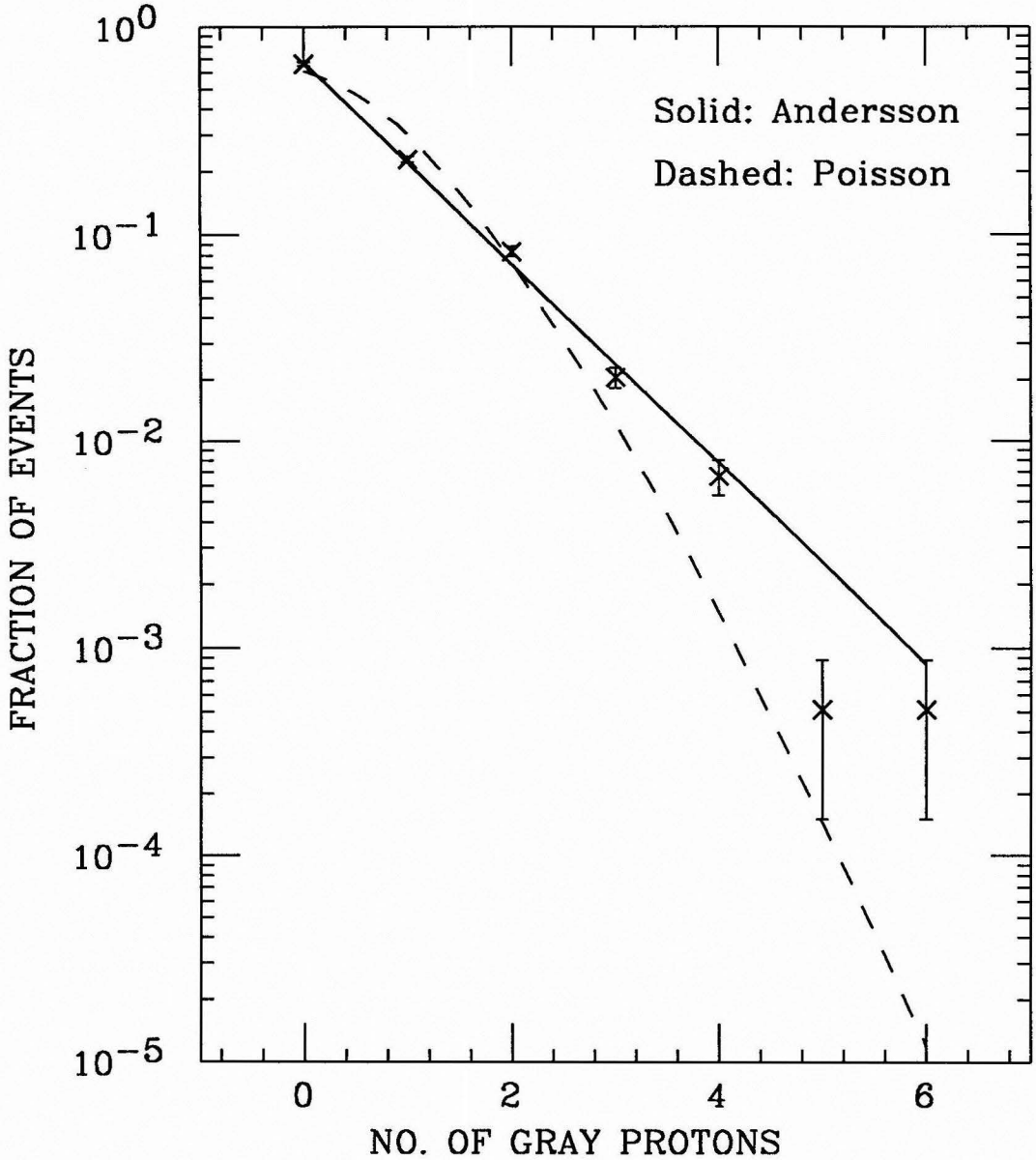

Figure 6.4: Fraction of events versus the number of gray protons in the events

Table 6.3: Average gray proton multiplicity vs. Q^2

$Q^2(\mathrm{GeV/c})^2$	$< N_p > CC$
0-10	$.542 \pm .018$
10-40	$.475 \pm .018$
> 40	$.389 \pm .023$

Table 6.4: Average gray proton multiplicity vs. W^2

$W^2(\mathrm{GeV/c^2})^2$	$< N_p > CC$
0-100	$.502 \pm .014$
100-200	$.472 \pm .026$
>200	$.399 \pm .032$

from strictly backward protons, it is worth mentioning that a decrease in backward gray proton multiplicity versus Q^2 was observed in Ref.[5]. We have mentioned in the introduction that only low energy particles get the chance to reinteract in the nucleus, since high energy particles are formed outside of the nucleus. However, intuitively we may think of a competing process: when more energy is available to the hadronic sector, the number of particles would also increase, possibly resulting in an increased production of protons due to intranuclear cascade. However, when we examine Figures 6.5 and 6.6, we see that the mean energy of a hadron in an event increases with Q^2 and W^2 of the event. The increase means that with increased energy available to the hadronic system, generally fewer low energy particles are produced. Since it is the lower energy particles which undergo rescattering, rescattering is produced more often in events with lower energy available to the hadronic system. These results are consistent with the hypothesis of finite fomation length which has been observed in hadron-nucleus experiments[1, 3].

6.2 Backward Particle Production and the Rescattering Model

In our proton sample derived from all the events there are 820 backward gray protons. They make up a significant 19% part of the whole. Their momentum is too high for them to be produced by evaporation of the nucleus. On the other hand, a backward

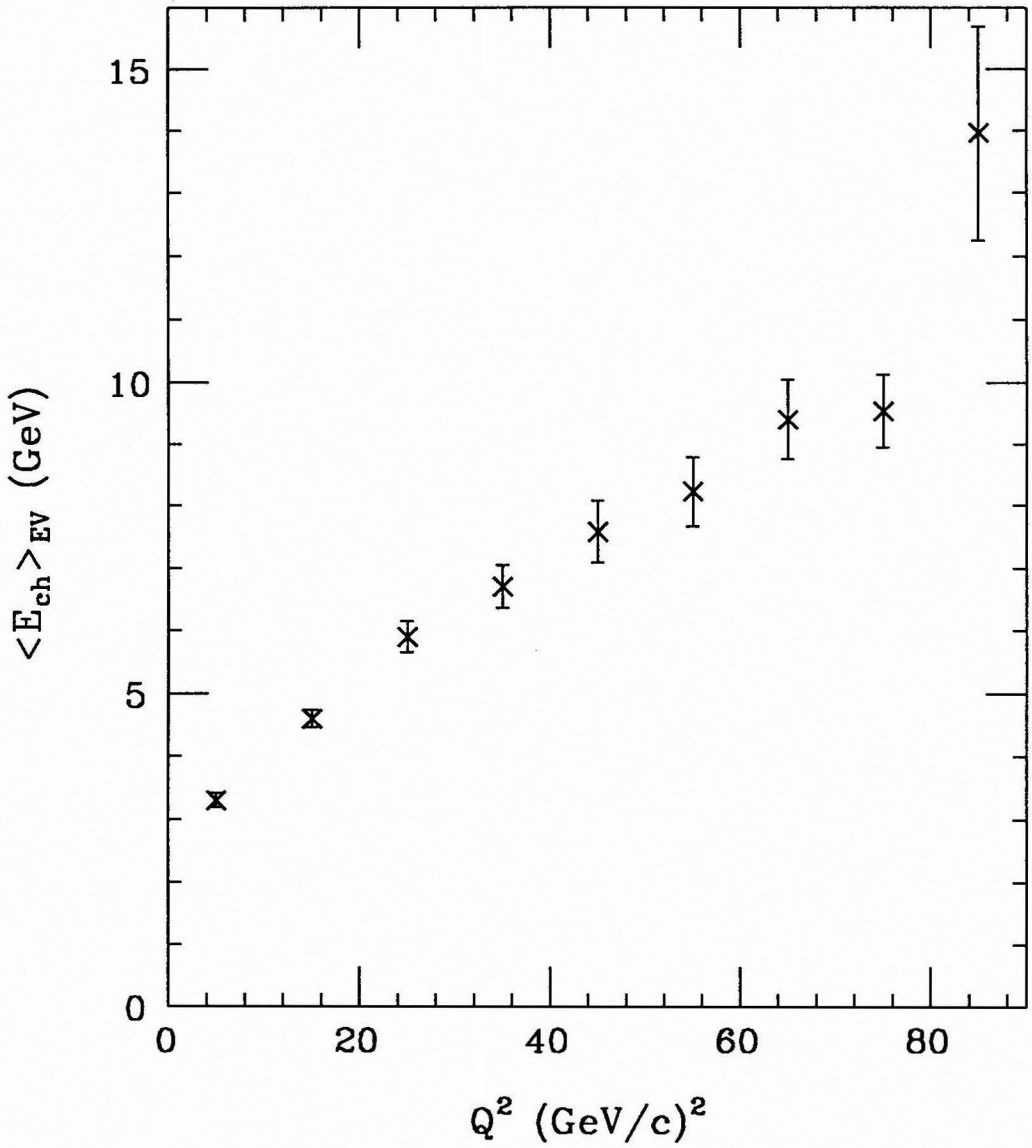

Figure 6.5: Mean energy per hadron (not including black protons) vs. Q^2 per event

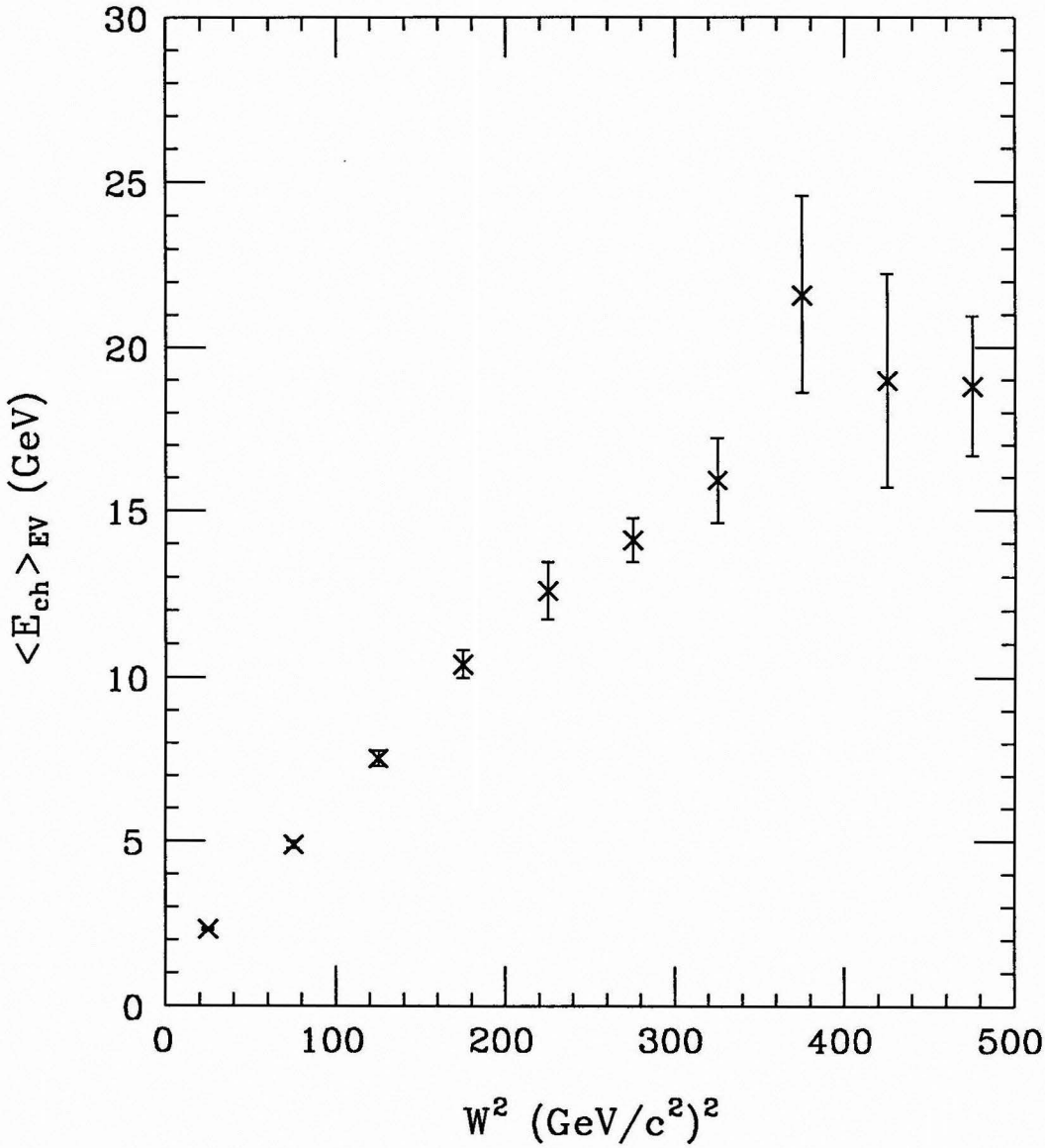

Figure 6.6: Mean energy per hadron (not inluding black protons) vs. W^2 per event

proton cannot be produced by a single scatter off a free nucleon target due to momentum and energy conservation. The presence of these backward protons implies that there is a nuclear effect taking place, such as some clustering of nucleons inside the nucleus(see section 2.3). Scattering could occur off of these clusters producing backward protons.

In Figure 6.7 we plotted the mean number of backward protons versus the number of forward protons, i.e. taking all events with a given number of forward protons we calculated the mean number of backward protons. We observe a rise which is approximately linear. The linearity of this rise is discussed in Refs.[4, 6, 14]. In Ref.[4] it is argued that the backward proton multiplicity is proportional to the number of intranuclear collisions. Since many of the forward protons are produced by secondary collisions, the simplest explanation for the linear rise is that since secondary protons are weakly correlated and their momentum and angular distributions are the same regardless of the total number of protons in an event, events with a higher total number of protons are automatically more likely to also have more backward protons, see Ref.[14]. Our data agrees well with the plots in Ref.[4, 6], both of which used neutrino beams. The plot in Ref.[14] using a proton beam, though linear, has a larger slope than ours. Thus the backward protons could be produced by rescattering.

6.3 Pion Absorption

A specific type of rescattering which could produce backward protons is the absorption of slow pions by a nuclear cluster in the nucleus: $\pi + "b" \rightarrow N + N$ or $\pi + "b" \rightarrow \Delta + N$ with $\Delta \rightarrow \pi + N$, and "b" is assumed to be a two-nucleon cluster. Such a process is mentioned in Ref.[4], where the $< N_B >$ vs. N_F plot agrees well with a Monte Carlo simulation which includes $\pi + "b" \rightarrow N + N$ absorption, but doesn't agree with a simulation not including pion absorption.

The rate of π^+ absorption is known to be three times as high as π^- absorption. The cross section for the $\pi^+ d \rightarrow pp$ process has a peak at $p_\pi \approx 0.25$ GeV/c. The solid curve in Figure 6.8 shows the shape of the cross section, from Ref.[6]. In the figure we plotted the mean ratio of N_{π^-} to N_{π^+} in bins of π momentum for three cases. Notice that for events with backward protons we see more depletion of π^+ production in the

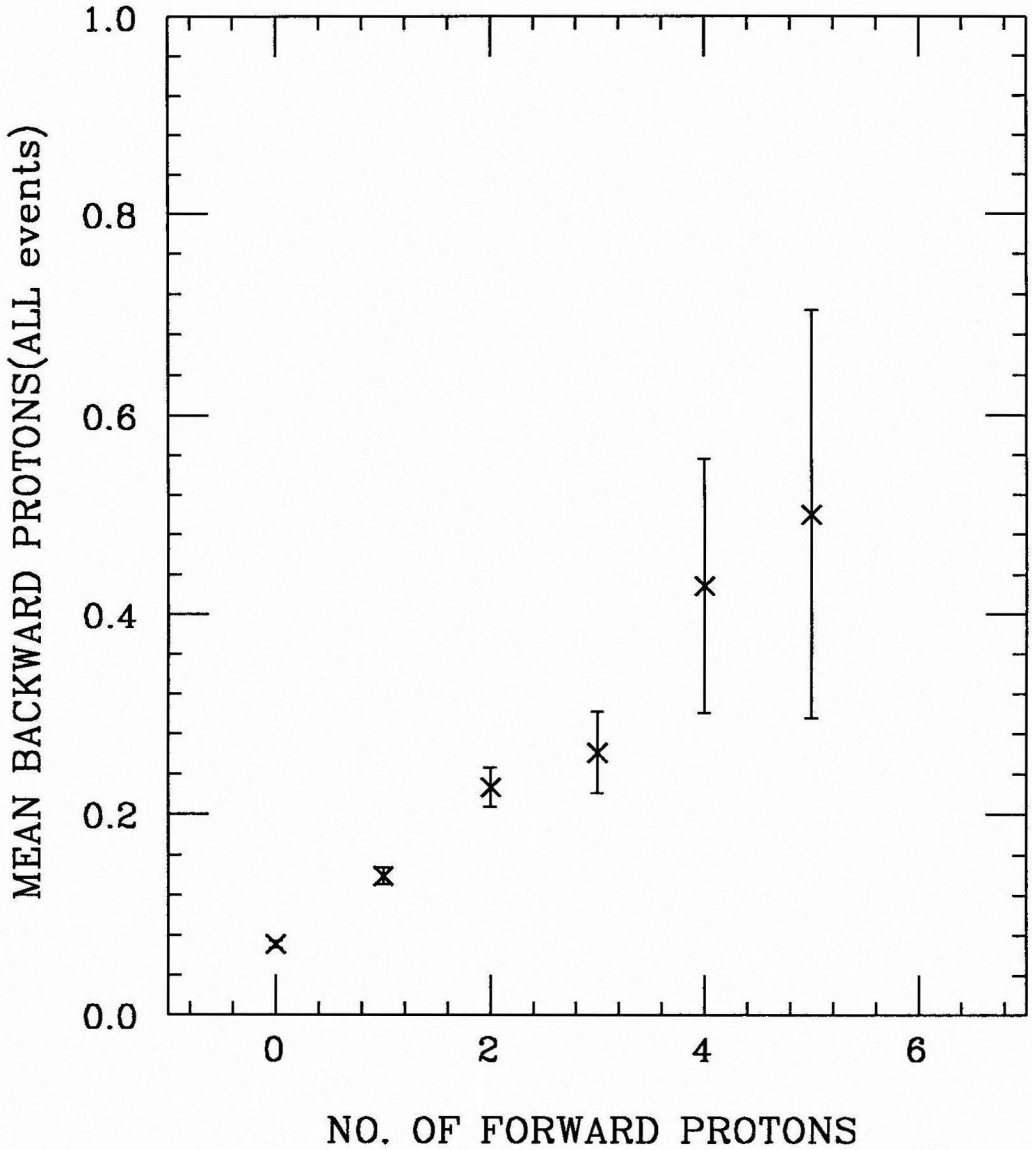

Figure 6.7: Mean backward gray proton multiplicity versus forward gray proton multiplicity

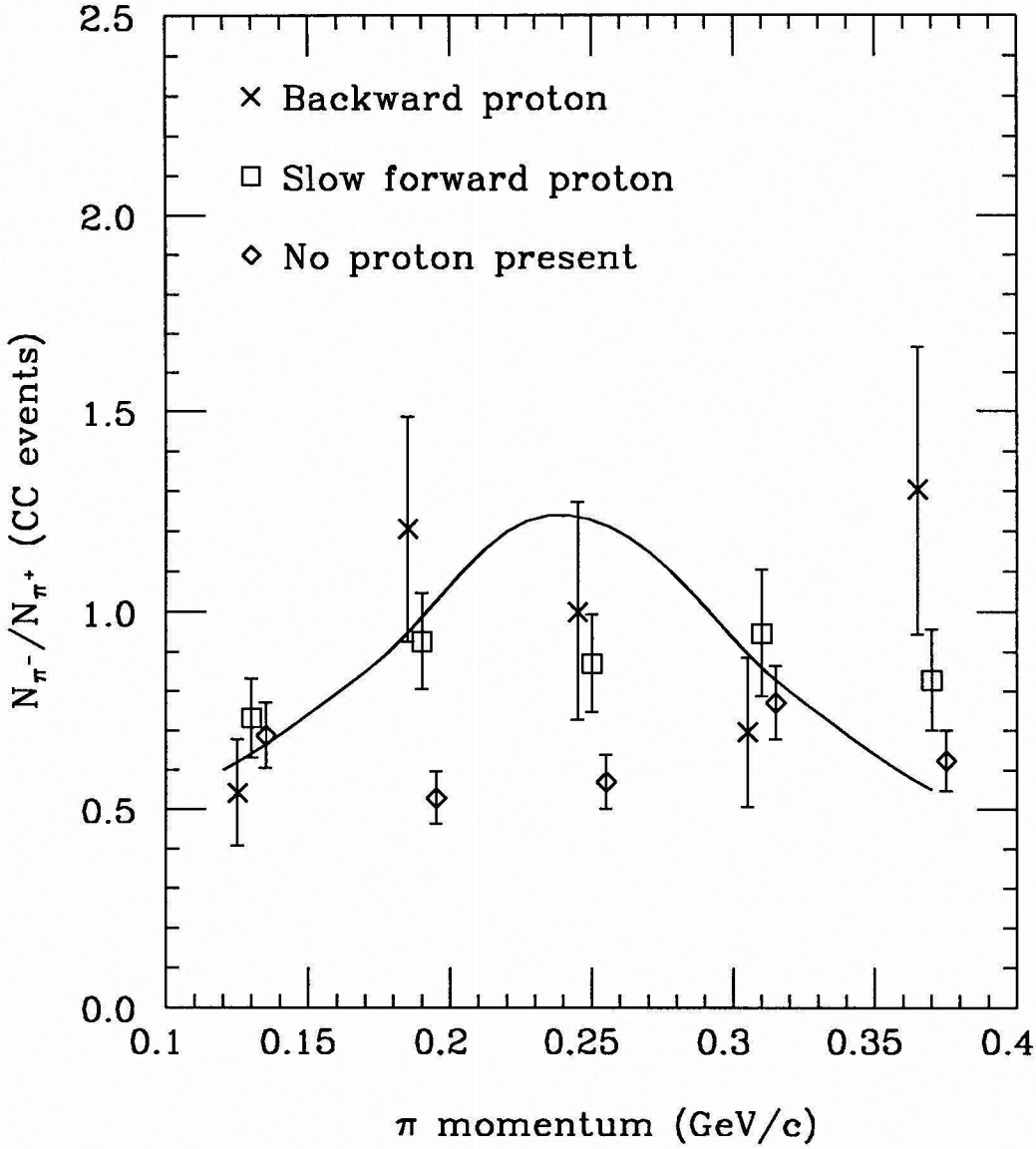

Figure 6.8: Ratio of negative pion multiplicity to positive pion multiplicity in pion momentum bins. The solid curve shows the shape of the $\pi^+ d \rightarrow pp$ cross section

range of .20 – .25 GeV/c than for events without any protons. Since pion absorption can also produce forward protons, we included them in this plot as a separate case, in the momentum range of the backward protons (.30 to .80 GeV/c). There is a similar depletion indicating pion absorption.

6.3.1 Evidence for $\pi + "b" \rightarrow N + N$ Mechanism

In Ref.[14] a kinematical variable

$$\mu^2 \equiv (T_1 + T_2)^2 - (\vec{p}_1 + \vec{p}_2)^2 \tag{6.14}$$

is defined for the reaction $\pi + "b" \rightarrow p_1 + p_2$, where "$b$" represents a cluster of two nucleons, and T_1 and T_2 are the kinetic energies of the outgoing protons. A signal in this variable is claimed to give direct evidence for the existence of this process. μ^2 comes from a four-vector analysis of the above reaction where the pion and the "b" system are nearly at rest.

$$\begin{aligned}
(E_\pi + E_b)^2 - (\vec{p}_\pi + \vec{p}_b)^2 &= (E_1 + E_2)^2 - (\vec{p}_1 + \vec{p}_2)^2 && (6.15)\\
(m_\pi + 2m_p)^2 &\approx (T_1 + T_2 + 2m_p)^2 - (\vec{p}_1 + \vec{p}_2)^2 && (6.16)\\
m_\pi^2 + 4m_p m_\pi + 4m_p^2 &= 4m_p^2 + 4m_p(T_1 + T_2) \\
&\quad +(T_1 + T_2)^2 - (\vec{p}_1 + \vec{p}_2)^2 && (6.17)\\
m_\pi^2 + 4m_p m_\pi - 4m_p(T_1 + T_2) &= (T_1 + T_2)^2 - (\vec{p}_1 + \vec{p}_2)^2 \equiv \mu^2 && (6.18)
\end{aligned}$$

Energy conservation:

$$\begin{aligned}
E_\pi + E_b &= E_1 + E_2 && (6.19)\\
m_\pi + 2m_p &= T_1 + T_2 + 2m_p && (6.20)\\
m_\pi &= T_1 + T_2 && (6.21)
\end{aligned}$$

Substituting m_π for $T_1 + T_2$ in equation (6.5), we find

$$m_\pi^2 \approx (T_1 + T_2)^2 - (\vec{p}_1 + \vec{p}_2)^2 = \mu^2. \tag{6.22}$$

We expect a broad peak in μ^2 shifted to the left of m_π^2 due to Fermi motion and the binding energy of the "b" system. In order to plot μ^2 in any event we made all proton

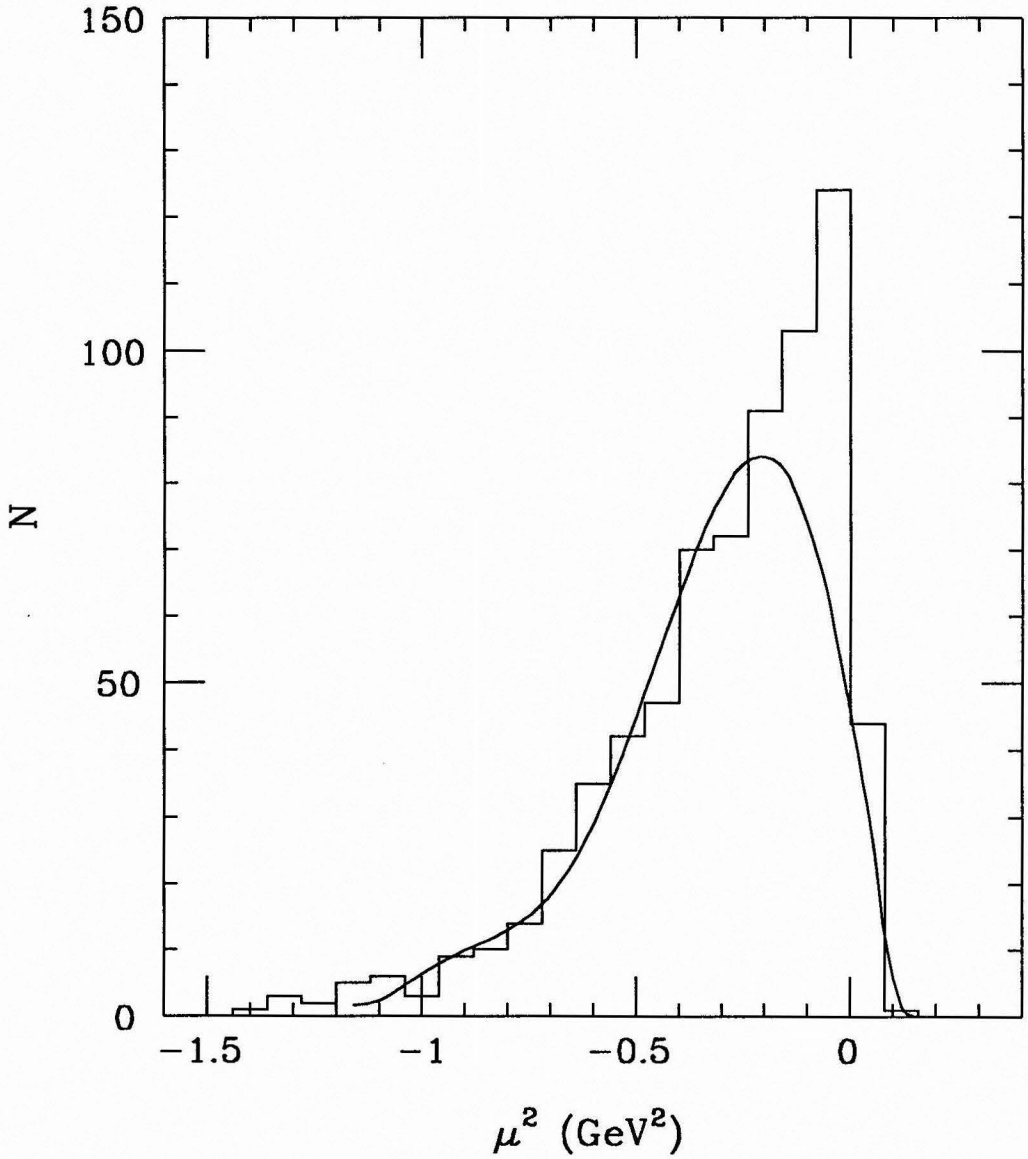

Figure 6.9: μ^2 for events with at least one backward proton. The solid line shows a polynomial fit to the background.

combinations for which at least one proton was backward, see Figure 6.9. We observe a peak near 0 GeV^2 (consistent with Ref.[14]), which shows a significant signal over background represented by the solid line. To generate the background we first saved the pairs of protons in the plot and then randomly combined the first proton of each pair with the second proton of another pair which was randomly selected 10 times. The background curve was normalized to the region below -0.4 GeV^2 and was fitted to a sixth order polynomial. Thus the μ^2 variable has been useful in showing that the pion absorption mechanism: $\pi + "b" \rightarrow N + N$ contributes to the production of backward protons.

6.3.2 Evidence for $\pi + "b" \rightarrow \Delta + N$ Mechanism

To examine whether backward protons could be produced by the production of resonances, $\Delta^0(N^*)$ with $M(p\pi^-)$ or Δ^{++} with $M(p\pi^+)$, we plotted the effective masses of these systems. Figures 6.10 and 6.11 show the $(p\pi^+)$ and $(p\pi^-)$ mass distributions respectively, where the pion has an angle in the backward hemisphere, and the proton has no restrictions on its angle. Although we do not see a Δ signal, the data can be fitted to be consistent with about 15-20% production of Δ^{++} and Δ^0. The fits were done to these plots using a polynomial background and a Breit-Wigner shape for the Δ using the world-average values of the Δ mass(1232 MeV/c^2) and width(120 MeV/c^2). All fits had good χ^2 per degree of freedom. The solid lines in the figures show the results of the fits, while the dashed lines indicate the background. Figures 6.12 and 6.13 show the same distributions with the same method of fitting, but the production angles of both pion and proton are in the backward hemishpere. Table 6.5 shows the numbers and rates of production for the resonances which are consistent with the results in Ref.[14]. The N* resonance which appears clearly though at lower rate than the Δ's in their experiment doesn't play a significant role in our experiment. They also noted that when both the proton and the pion for which the effective mass was plotted were backward, then the rate of Δ production increased. We also notice a tendency of increase in the rate, but the difference is only about one standard deviation. We conclude that the mechanism of Δ resonance production in $\pi + "b" \rightarrow \Delta + N$ with

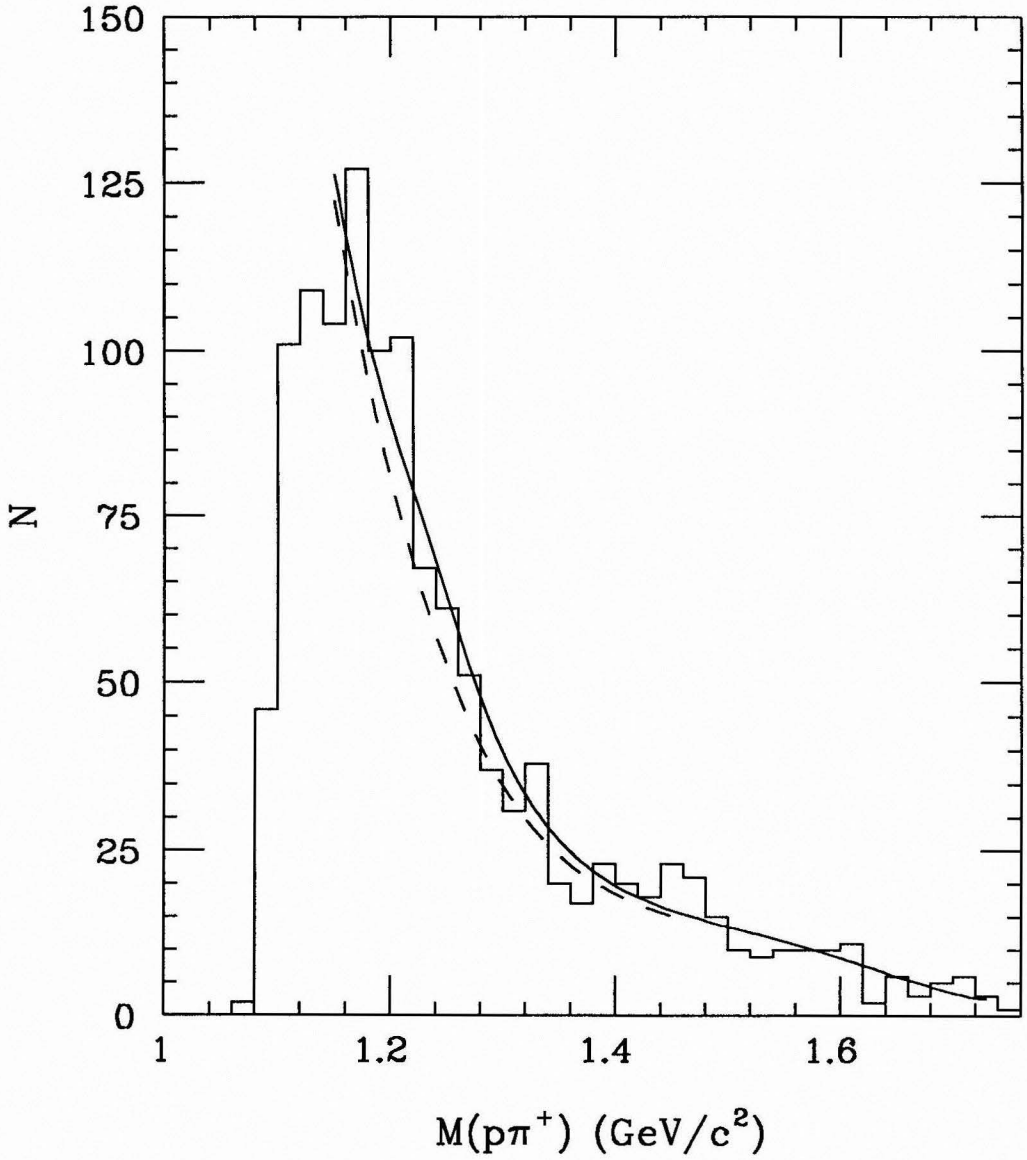

Figure 6.10: $M(p\pi^+)$ using backward pion with any gray proton

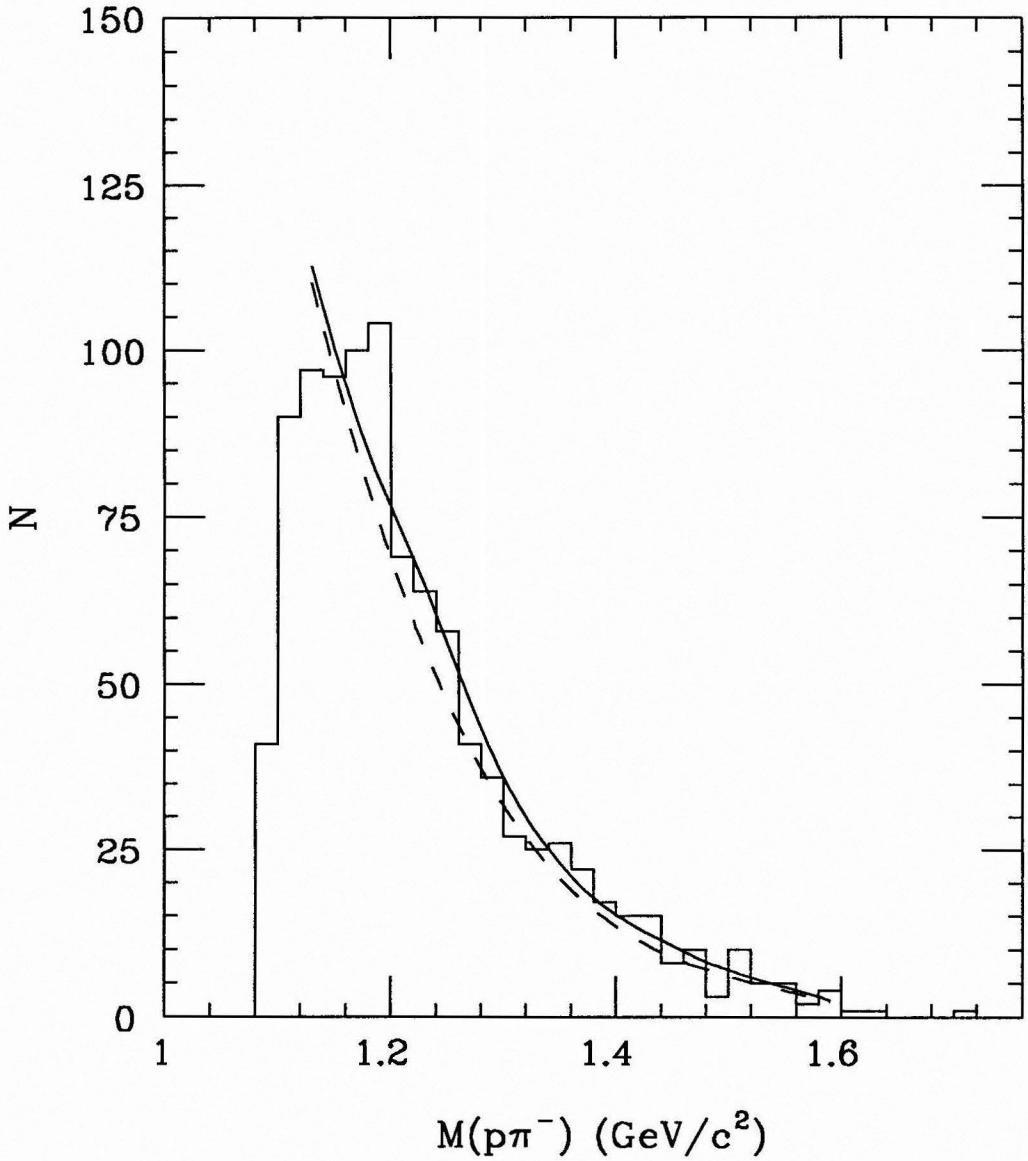

Figure 6.11: $M(p\pi^-)$ using backward pion with any gray proton

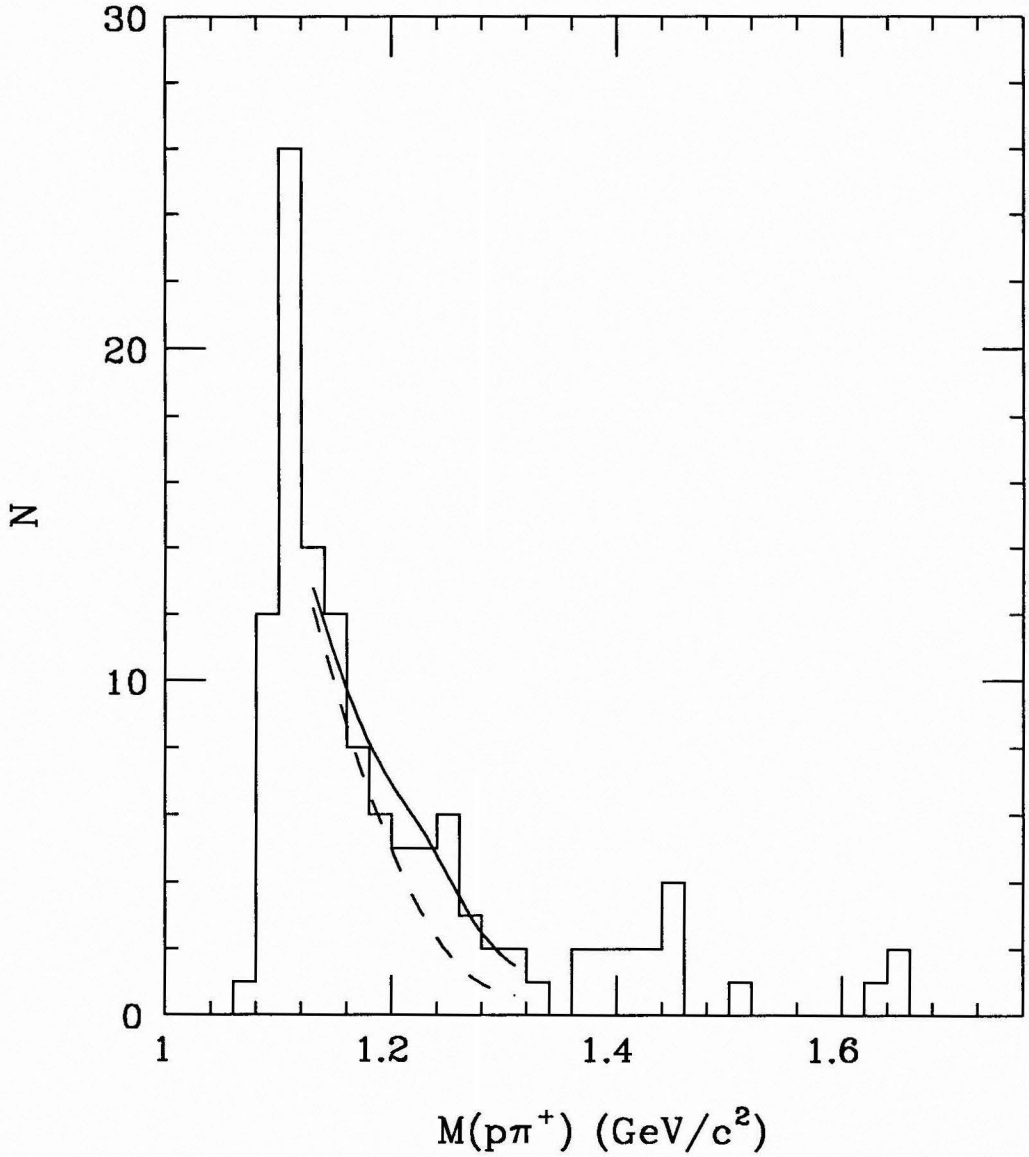

Figure 6.12: $M(p\pi^+)$ using backward pion with backward gray proton

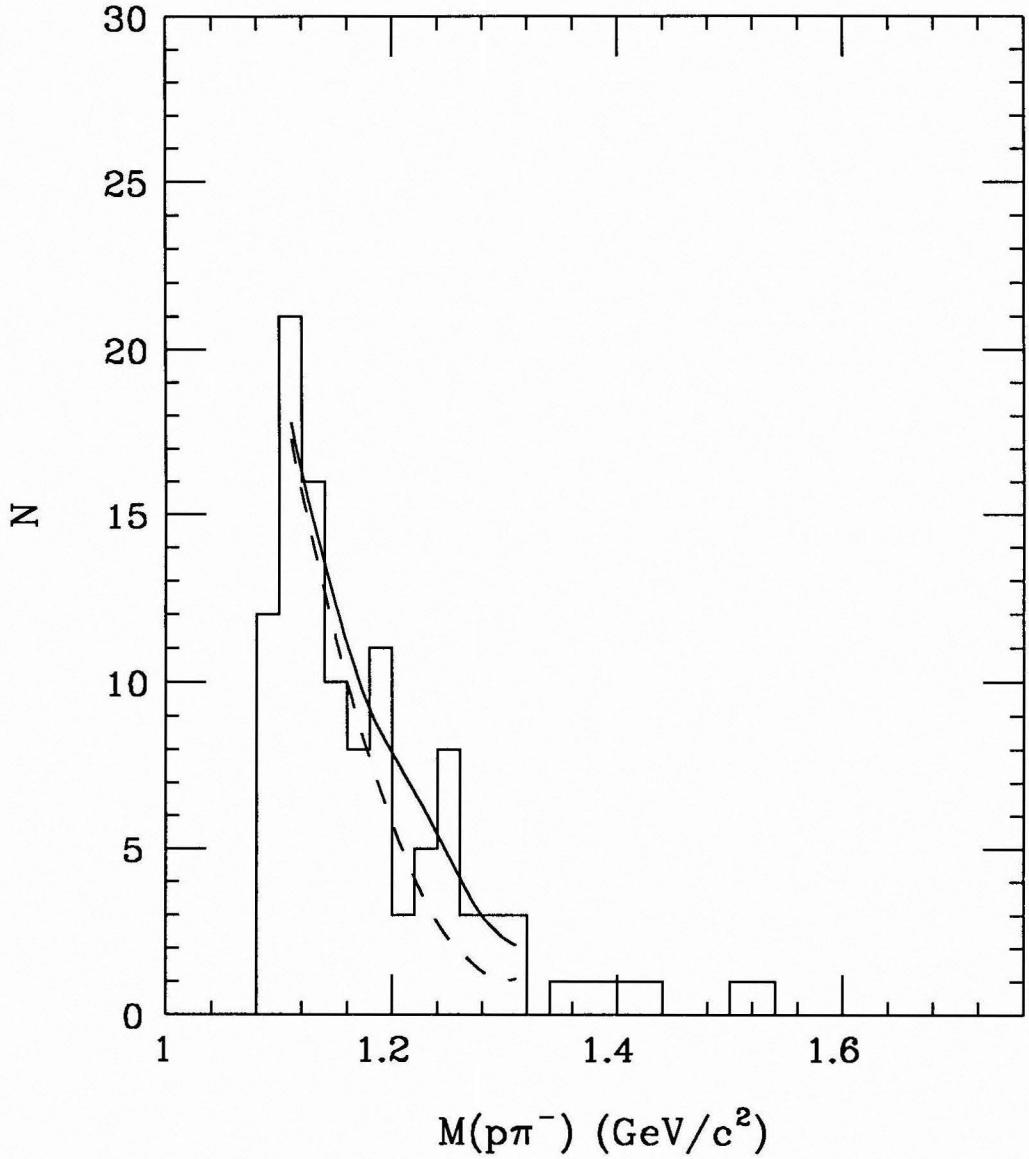

Figure 6.13: $M(p\pi^-)$ using backward pion with backward gray proton

Table 6.5: Delta resonances

Figure	# of Events	Resonance	N(res.)	Rate
6.10	750	Δ^{++}	83 ± 20	$(11 \pm 3)\%$
6.11	584	Δ^{0}	72 ± 19	$(12 \pm 3)\%$
6.11	584	N^{*}	8 ± 8	$(1.4 \pm 1.4)\%$
6.12	103	Δ^{++}	16 ± 5	$(16 \pm 5)\%$
6.13	93	Δ^{0}	18 ± 6	$(19 \pm 6)\%$

$\Delta \rightarrow \pi + N$ plays a significant part in the production of backward protons.

In Ref.[14] the plot of the μ^2 variable shows a signal for Δ production in addition to a signal for the process $\pi + "b" \rightarrow N + N$. We earlier discussed that the peak near $\mu^2 \approx 0$ GeV^2 refers to the latter process. In addition to this peak they find another peak at $\mu^2 \approx -0.22$ GeV^2. They claim that this peak which is shifted to the negative arises from the reaction $\pi + "b" \rightarrow \Delta + p_1$ with $\Delta \rightarrow p_2\pi$. To examine how this negative shift may take place we define

$$\mu_1^2 \equiv (T_1 + T_\Delta)^2 - (\vec{p}_1 + \vec{p}_\Delta)^2, \tag{6.23}$$

and we write an analagous equation to equation (6.18):

$$m_\pi^2 + 4m_p m_\pi - 4m_p(T_1 + T_\Delta) = (T_1 + T_\Delta)^2 - (\vec{p}_1 + \vec{p}_\Delta)^2 \equiv \mu_1^2 \tag{6.24}$$

In order to find the shift in μ^2, we subract the left hand side of equation (6.18) from the left hand side of equation (6.24). Thus:

$$\begin{aligned}
\mu_1^2 - \mu^2 &= 4m_p(T_1 + T_2 - T_1 - T_\Delta) && (6.25)\\
&= 4m_p(T_2 - T_\Delta) && (6.26)\\
&= 4m_p[T_2 - (E_\Delta - m_\Delta)] && (6.27)\\
&= 4m_p[T_2 - (T_2 + T_\pi + m_p + m_\pi - m_\Delta)] && (6.28)\\
&= 4m_p(m_\Delta - m_p - m_\pi - T_\pi) && (6.29)\\
&= 4m_p(0.154GeV - T_\pi). && (6.30)
\end{aligned}$$

Note that T_π is the kinetic energy of the pion produced by the Δ. Earlier in the resonance analysis we plotted the effective mass spectra of the Δ's with backward

pions only, so here we will also consider only the backward ones. Examining the above formula, we notice that no shift is produced for a pion with momentum .259 GeV/c, so for a negative shift the average pion momentum would have to be larger than this. We have plotted μ_1^2 in Figure 6.14 and $\mu_1^2 - \mu^2$ in Figure 6.15 using only the pions which gave an effective mass within the Δ width. We see a small signal in μ_1^2. The $\mu_1^2 - \mu^2$ plot shows a small positive shift. Thus we do not expect to see a negative shift in μ^2 as a signal to Δ production, we expect it to be absorbed by the main peak near 0 GeV^2. For completeness, in Figure 6.16 we plotted μ^2 with the restriction that there be no backward pions in the events. For Figure 6.17 we required that there be a backward pion in the event. In Ref.[14] similar plots were made, and it was observed that when backward pions were required, then the peak at $-.22$ GeV^2 was enhanced compared to when there were no backward pions allowed, suggesting that the peak shifted to the negative is indeed a signal for Δ resonance production. In our data no enhancement is observed, the peak in Figure 6.17 is near 0 GeV^2 and is about one standard deviation above the background.

The analysis of the μ^2 variable suggests that in our experiment the pion absorption process $\pi + "b" \rightarrow N + N$ dominates over $\pi + "b" \rightarrow \Delta + N$. From the analysis in this section we conclude that pion absorption plays a significant role in the production of backward protons.

6.4 The Two-Nucleon Correlation Model

A specific way to look for two-nucleon correlations is to study correlations between backward protons and the muon in CC events. The variables v_N and α have been described in section 2.3. Figures 6.18 and 6.19 show v_N versus α, where α is a kinematic variable associated with the spectator proton. The first plot is for all events with backward protons, note that many of these events have forward protons as well. The second plot is for events with only one proton which must be backward. The straight lines are the predictions of the two-nucleon correlation model. Ref.[6] showed that the $\nu - D_2$ plot was consistent with the model, and made comparisons using the $\nu - Ne$ data. For the first plot a small dependence on α was claimed, although all the points

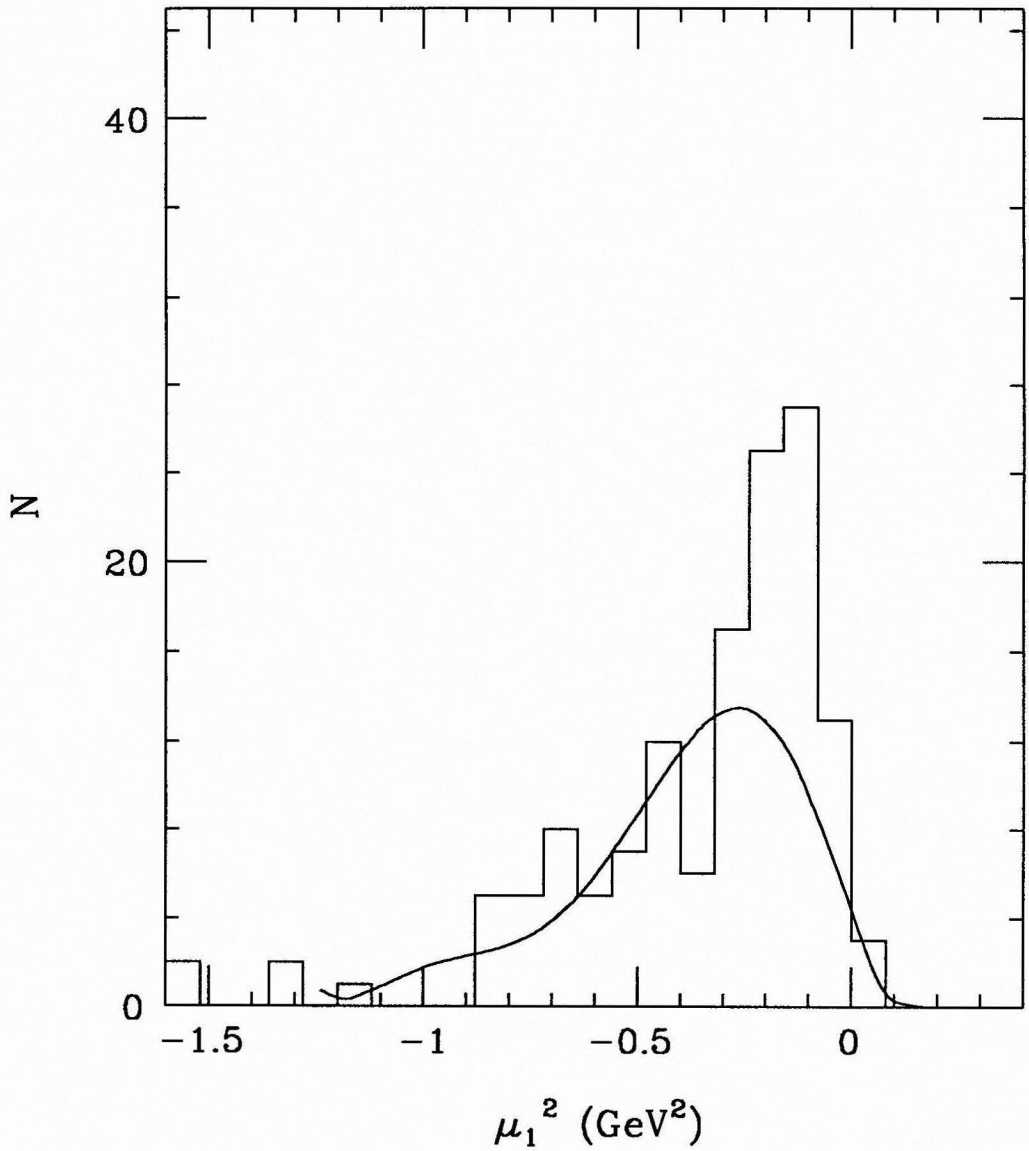

Figure 6.14: μ_1^2 using only backward pions which result in a Δ signal. The solid line shows a polynomial fit to the background.

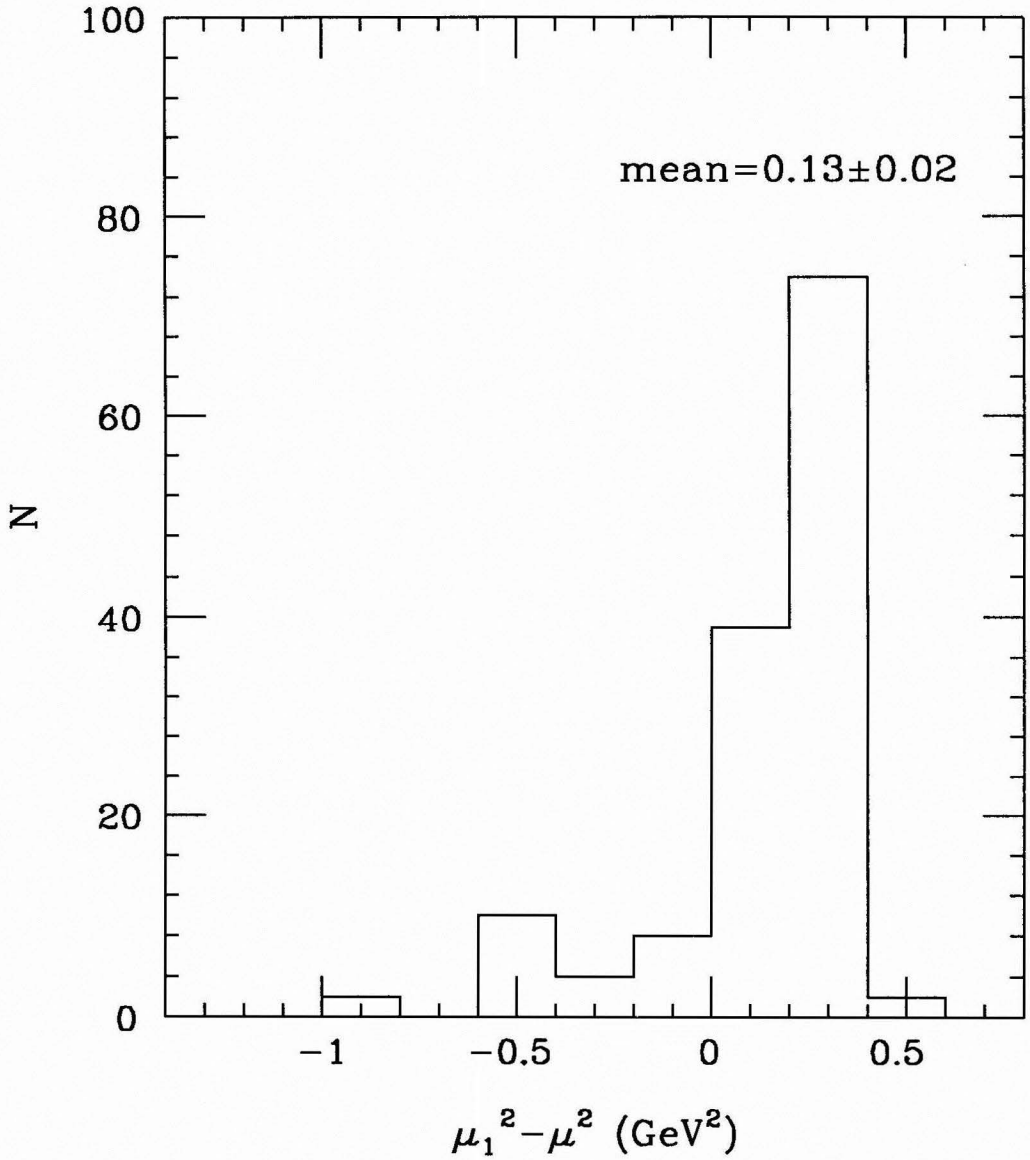

Figure 6.15: $\mu_1^2 - \mu^2$ (see equation (6.5)) using only backward pions which result in Δ signal.

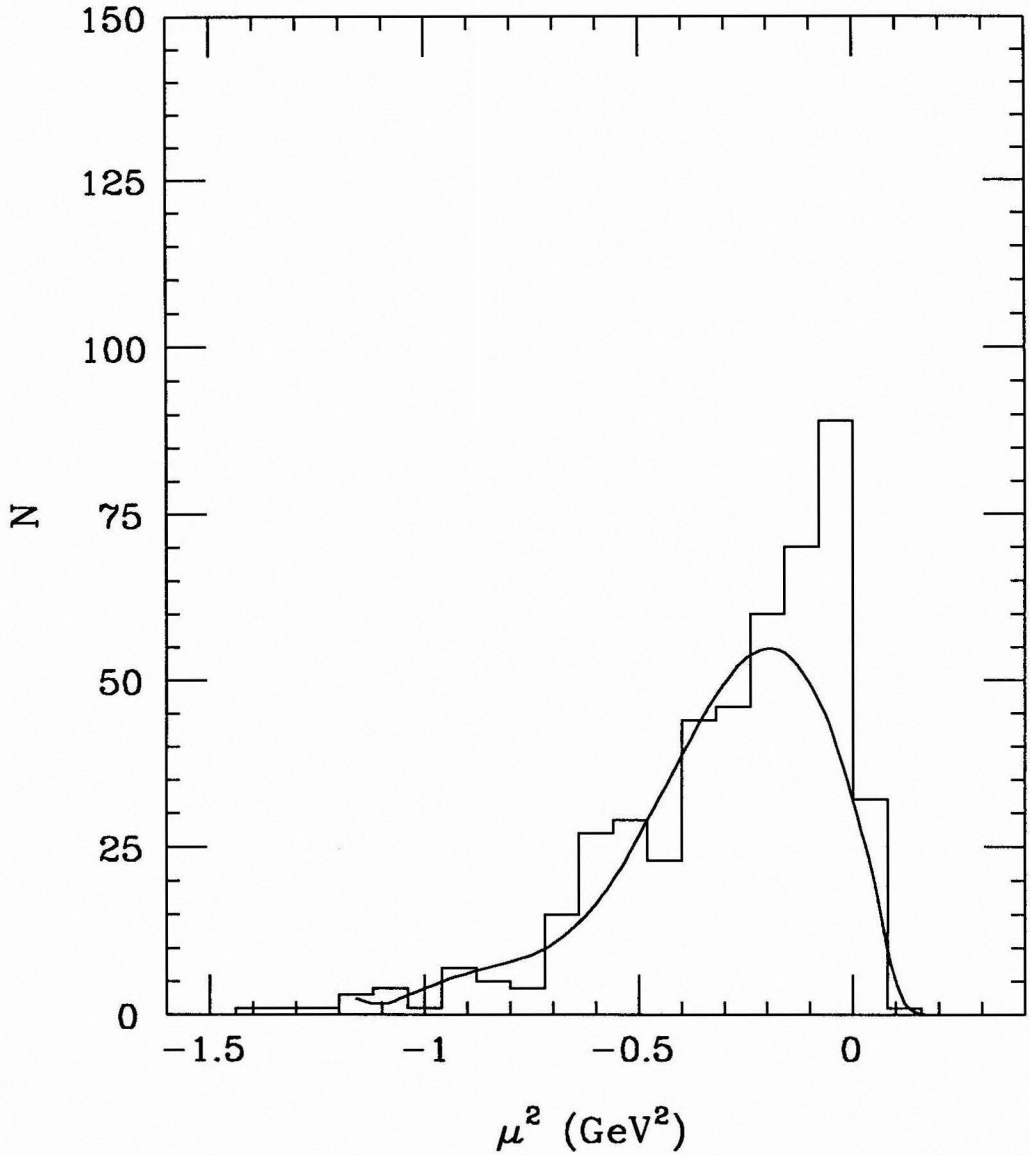

Figure 6.16: μ^2 for events with at least one backward proton and no backward pions. The solid line shows a polynomial fit to the background.

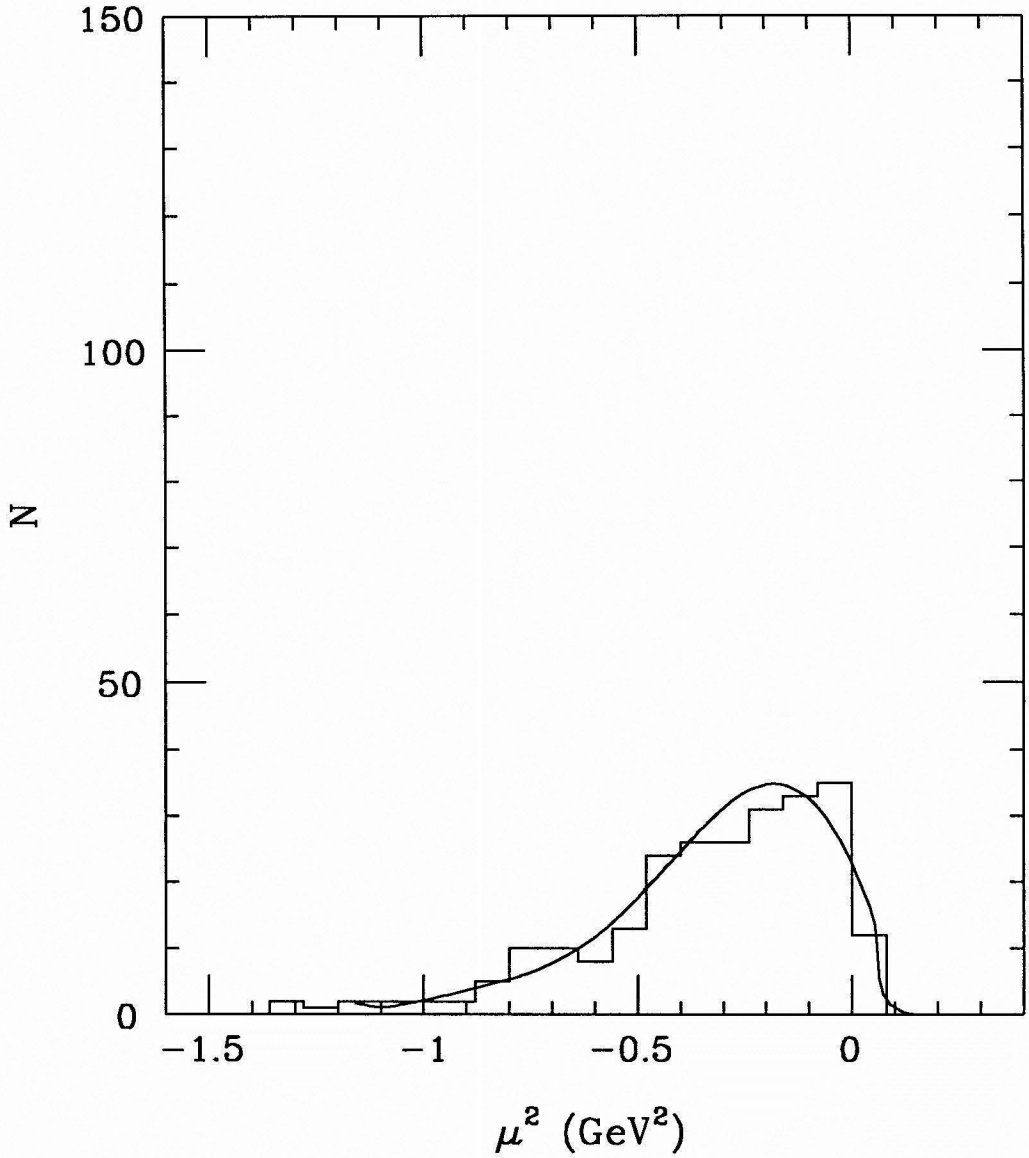

Figure 6.17: μ^2 for events with at least one backward proton and at least one backward pion. The solid line shows a polynomial fit to the background.

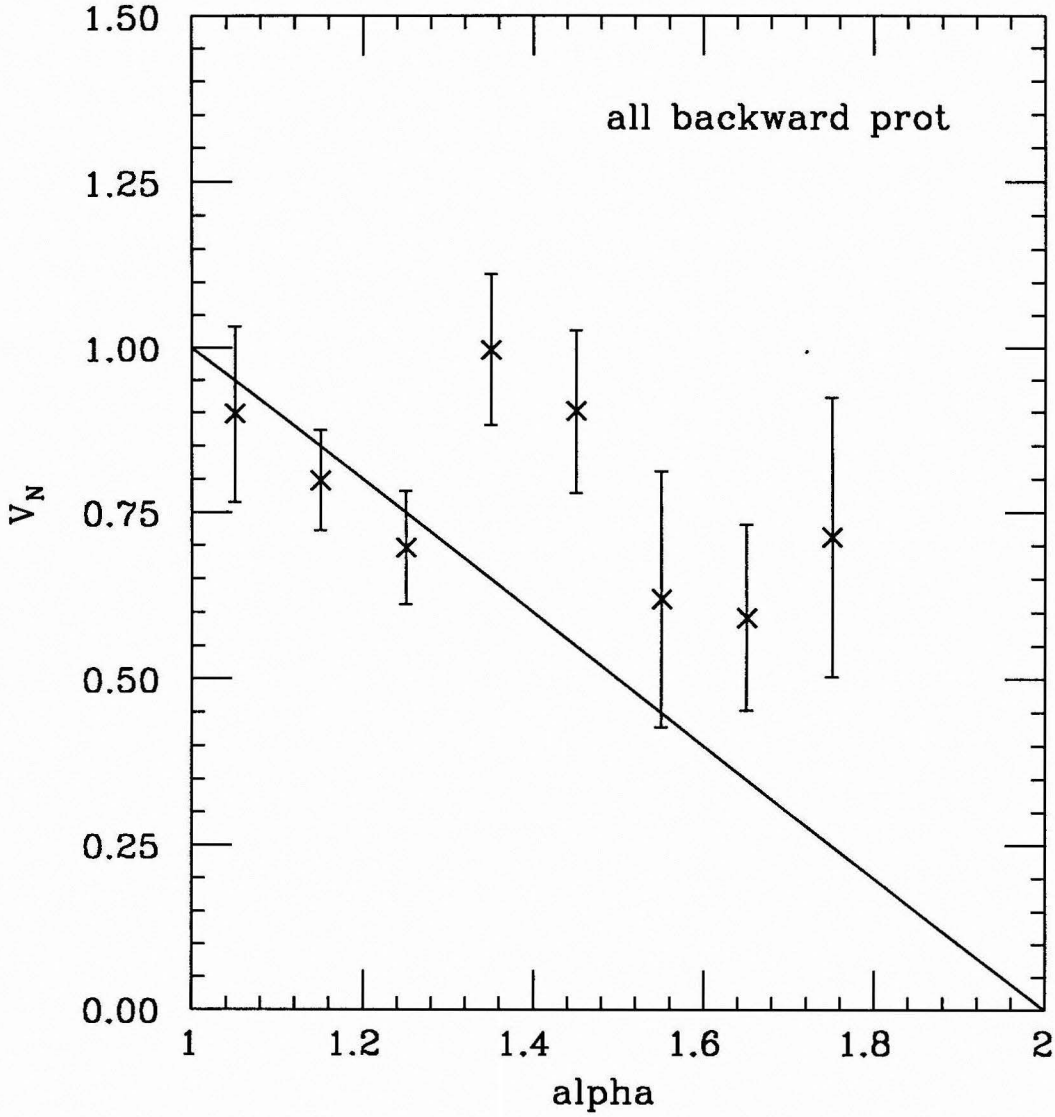

Figure 6.18: v_N vs. α for all events with at least one backward proton. The solid line shows the prediction of the SRO model.

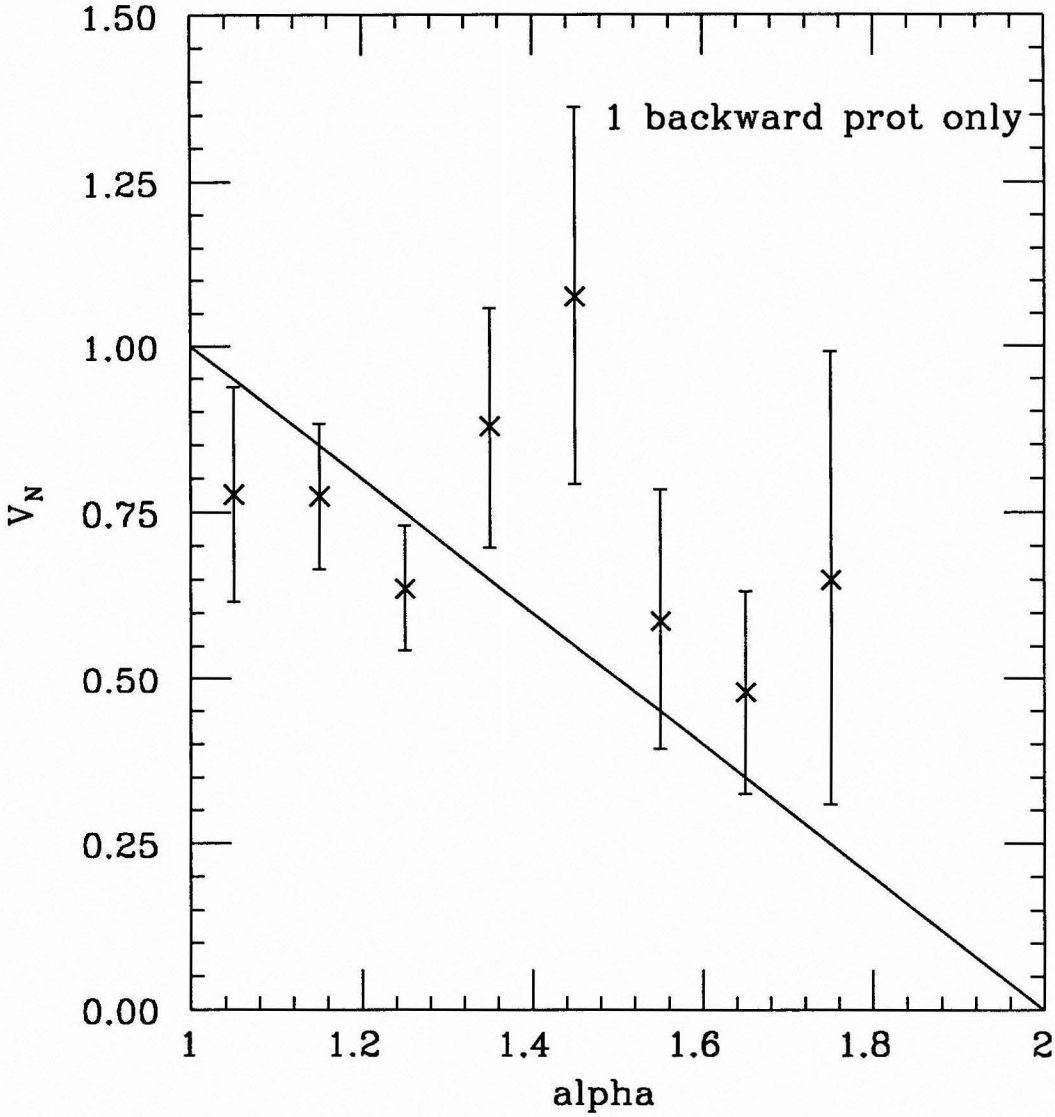

Figure 6.19: v_N vs. α for all events with only one backward proton and no other gray protons. The solid line shows the prediction of the SRO model.

Table 6.6: $B(\theta)$ slope parameter

	E632 $\nu - Ne$ $B(\mathrm{GeV/c})^{-2}$	E632 $(\nu\&\bar{\nu}) - Ne$ $B(\mathrm{GeV/c})^{-2}$	WA59[6] $(\nu\&\bar{\nu}) - Ne$ $B(\mathrm{GeV/c})^{-2}$	$(\nu\&\bar{\nu}) - D_2$ $B(\mathrm{GeV/c})^{-2}$
Backward p	11.02 ± 0.69	11.42 ± 0.65	10.69 ± 0.29	12.8 ± 2.0
1 backward p	11.53 ± 1.23	11.41 ± 1.10	11.2 ± 0.4	-
Backward π^+	5.87 ± 0.70	5.82 ± 0.64	9.0 ± 0.8	17.0 ± 3.0
Backward π^-	10.92 ± 1.33	12.03 ± 1.27	10.4 ± 0.8	14.0 ± 3.1

along with error bars were above the line predicted by the model. Our data shows a stronger correlation, although above $\alpha = 1.3$, v_N stays fairly consistently above the line. The second plot, for events with only one proton which must be backward, shows more of a decrease in v_N as α increases. The reason that the full sample of backward protons agrees less well with the correlation model is that in the events with protons other than one backward proton some rescattering takes place. The contribution from reinteractions is reduced for events with just one backward proton.

6.5 Backward Particle Differential Cross Section

In chapter 2 we noted that for backward protons the following differential distribution has been previously fitted successfully:

$$\frac{1}{N_{ev}} \frac{E}{p} \frac{dN}{dp^2} = C \exp(-B(\theta)p^2). \tag{6.31}$$

E and p are the energy and momentum of the backward particle. Figure 6.20 shows the distribution for all backward protons, and Figure 6.21 for backward protons when only that one proton is present in the event. Figures 6.22 and 6.23 show the same distributions for backward positive and negative pions. The fitted slopes, $B(\theta)$, are shown in Table 6.6. Ref.[6], a $\nu - Ne$ experiment, found that the slopes were independent of the type of backward particle, and that they were consistent with the slopes found from $\nu - D_2$ data. The consistency with $\nu - D_2$ data may give evidence that two-nucleon clusters exist in Neon nuclei, however, we do not know how strong an indication this is. Our results are consistent with the slopes found in Ref.[6], although our slope for the π^+ plot is lower. We do not think that the lower slope is due to anything more than

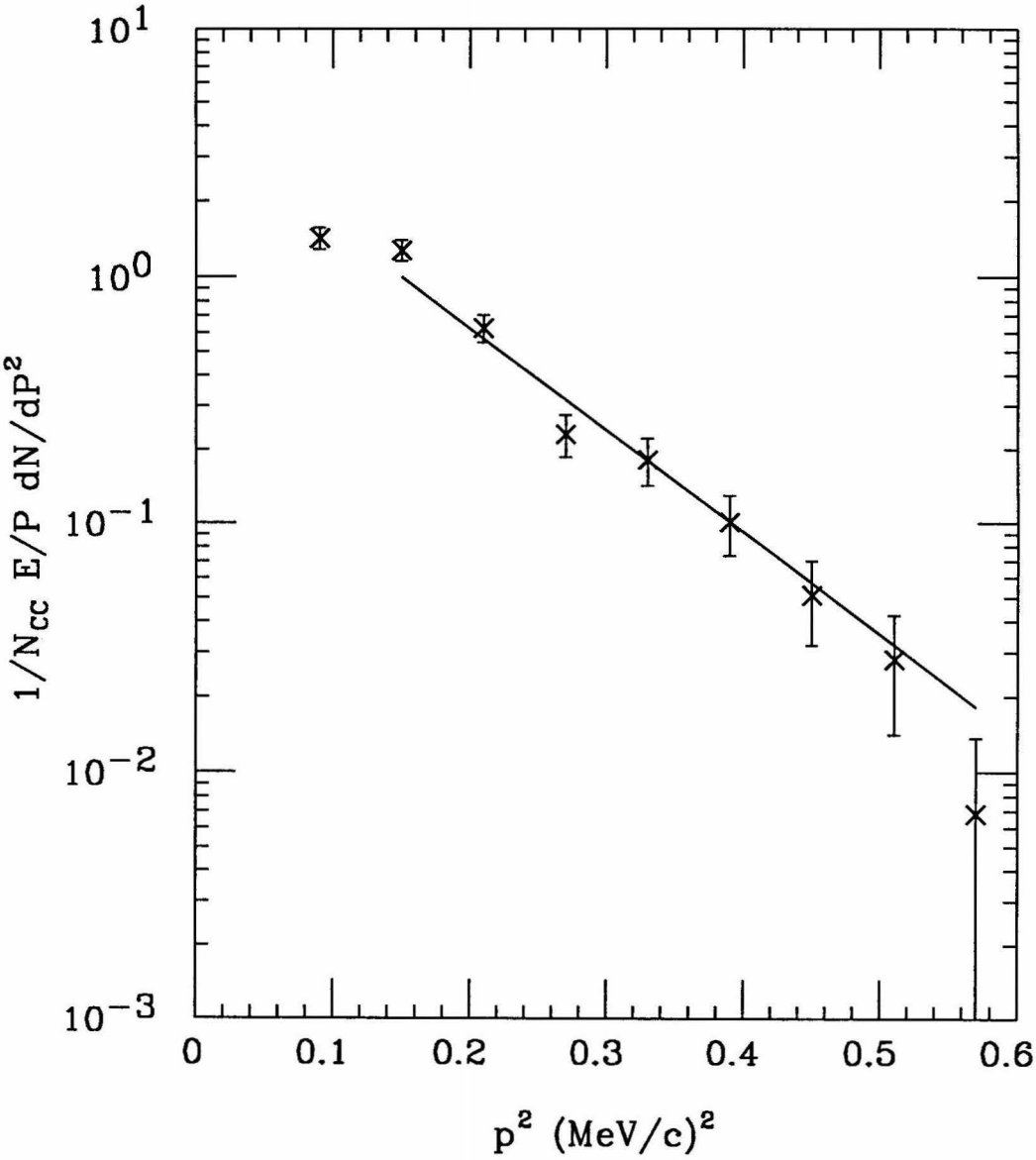

Figure 6.20: Differential distribution for backward protons

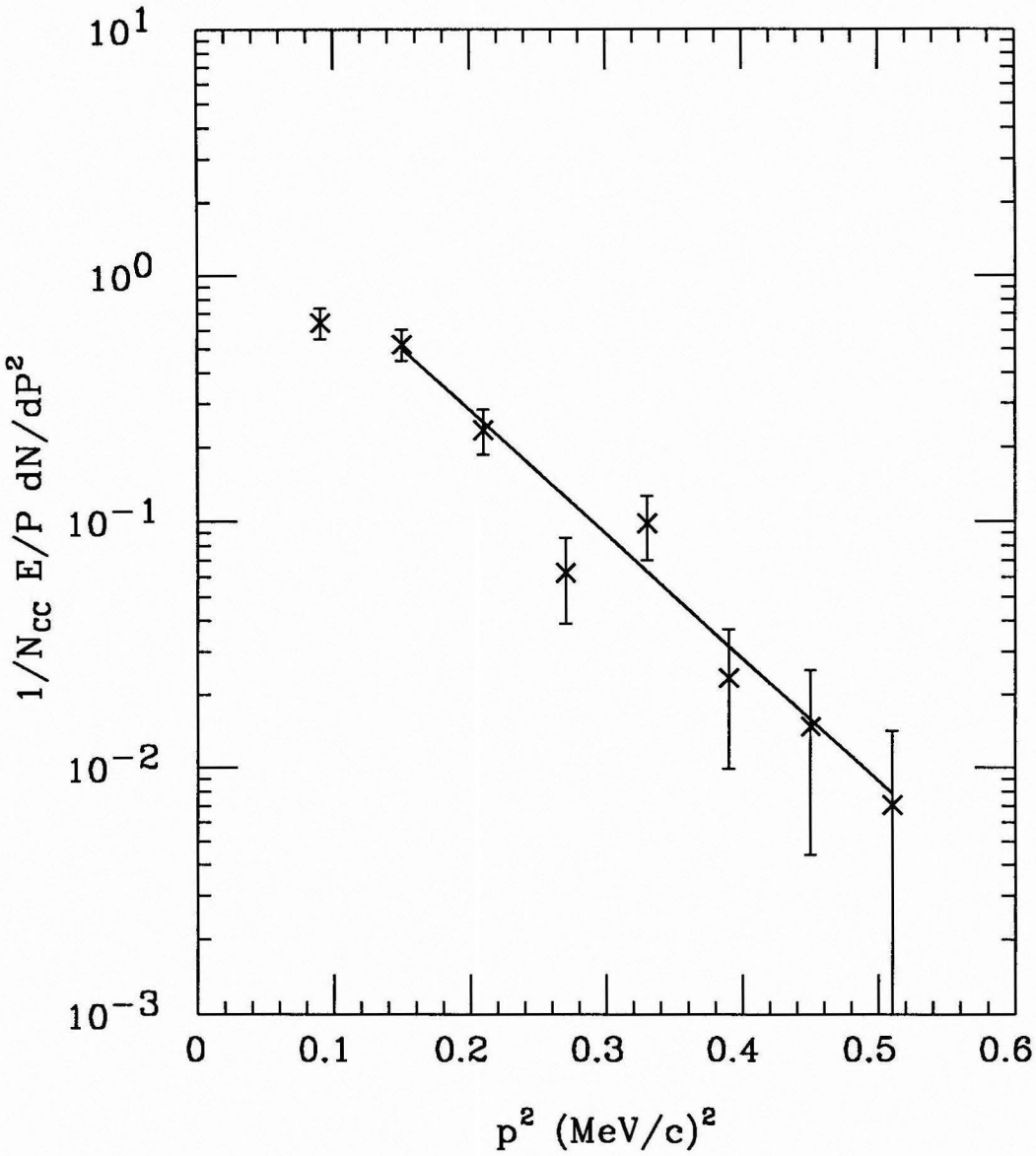

Figure 6.21: Differential distribution for backward protons in cases where the event contains only one backward proton and no other gray protons

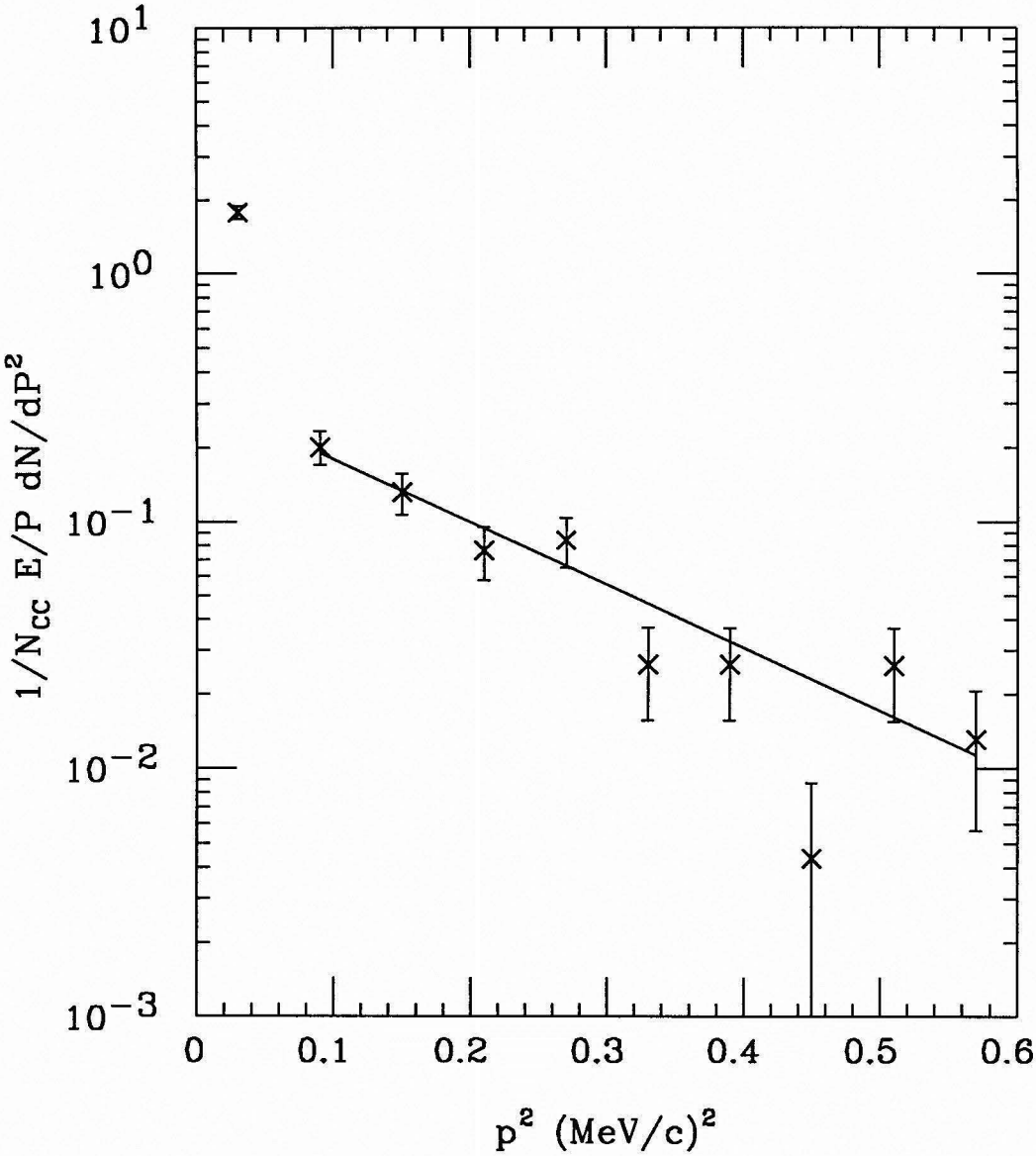

Figure 6.22: Differential distribution for backward π^+

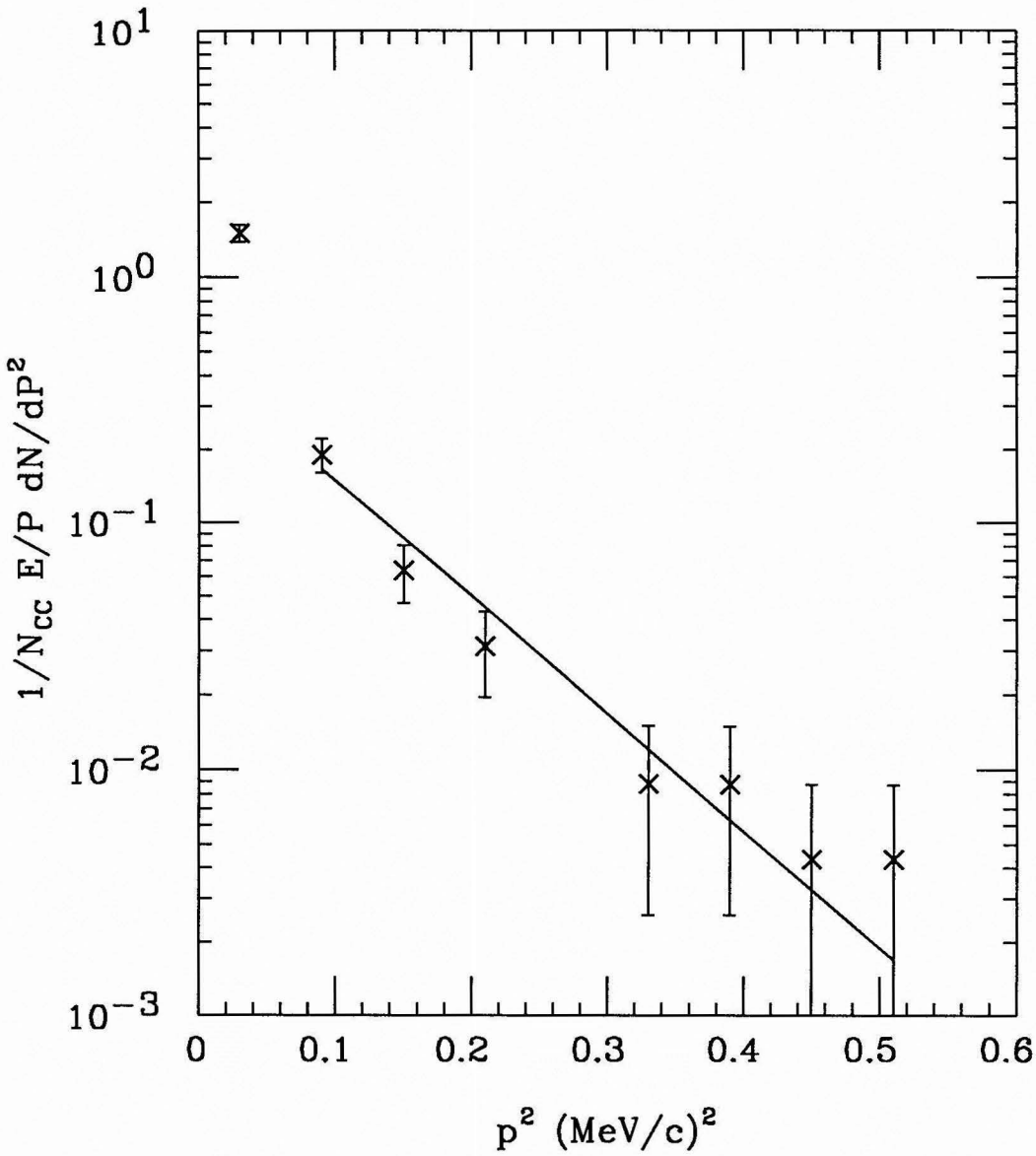

Figure 6.23: Differential distribution for backward π^-

statistical fluctuations. Figure 6.24 shows $B(\theta)$ plotted in bins of hadronic energy. We agree with previous experiments that the slope is independent of hadronic energy.

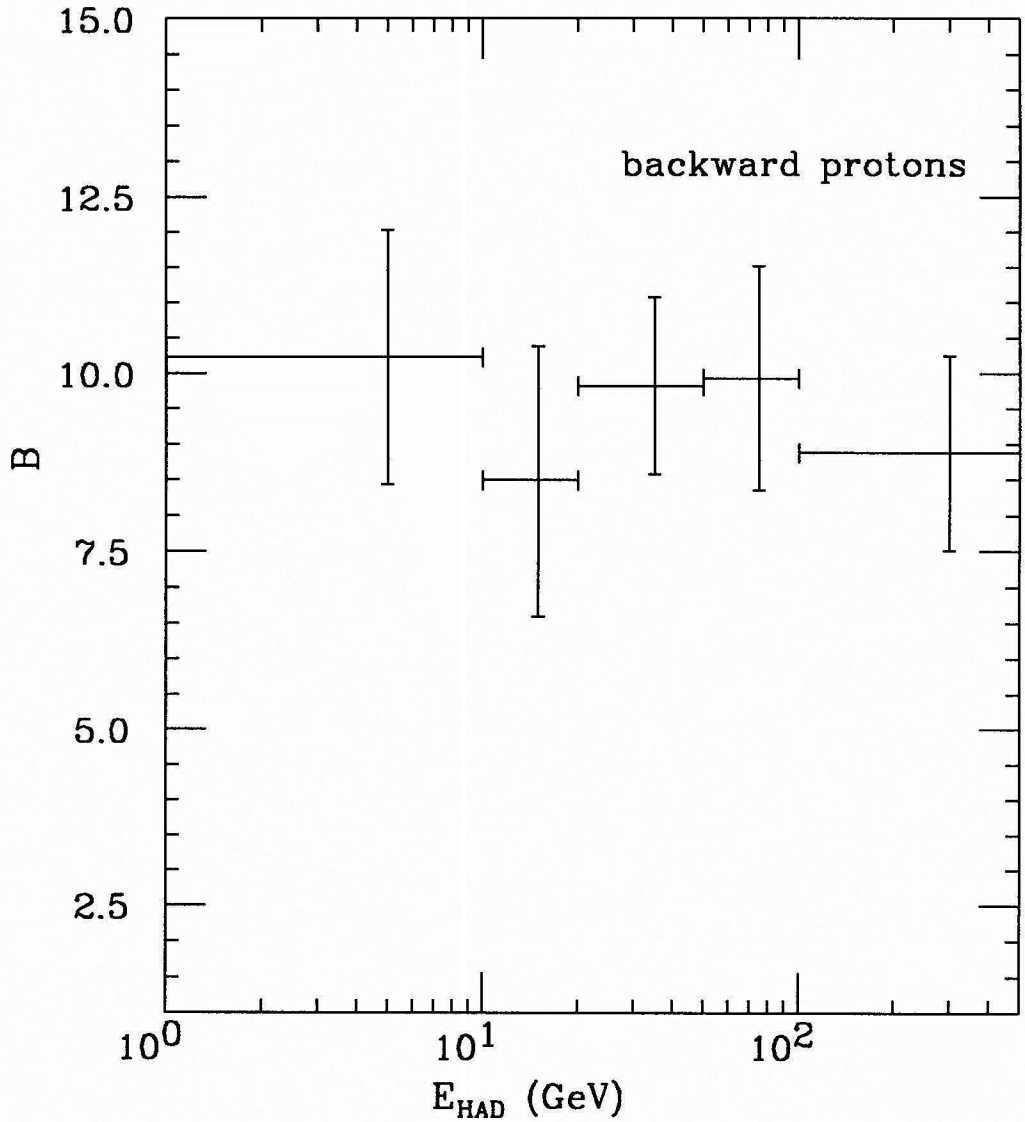

Figure 6.24: $B(\theta)$ vs. E_{HAD}

Chapter 7

Conclusions

In this thesis a study of proton production was done in $\nu -^{20} Ne$ interactions in the 15 ft. Bubble Chamber at the Tevatron. Muons were identified with the EMI and IPF systems of proportional tubes. A total of 8489 events were selected for analysis, 3898 of which were CC, 738 $C\bar{C}$, and 3853 NC.

Proton production has been previously studied in high energy hadron-nucleus experiments. Evidence has been found for an intranuclear cascade process, where the recoiling nucleon from a projectile collision collides with other nucleons in the nucleus. We found that it is advantageous to study proton production with a neutrino beam, because the neutrino interacts only once in the Neon nucleus, and the outgoing muon or neutrino does not reinteract. The average net charge in CC events was observed to be 0.73 ± 0.02. The expected net charge without rescattering was 0.34 ± 0.01. The origin of net charge excess was investigated. The mean number of gray protons ($300 \leq p \leq 1200$ MeV/c) was 0.49 ± 0.01 which was significantly higher than the number expected without secondary collisions: 0.25 ± 0.02. The fully corrected excess of gray protons is 0.34 ± 0.02. The net charge excess of 0.39 ± 0.02 was consistent with being made up of gray protons which were produced by secondary collisions during the intranuclear cascade, with the mean number of secondary collisions of 0.78 ± 0.04. A linear rise of the mean charge excess versus the number of gray protons with a slope of 0.73 ± 0.03 was observed. The ratio of the same quantities averaged over the whole sample is 0.80 ± 0.04, which is consistent with the slope, and indicates that the charge excess is made up of gray protons. The fractional distribution of gray protons is well described by the model of Andersson, Otterlund and Stenlund which is derived from a Glauber calculation with a Woods-Saxon nucleon density distribution. The Poisson distribution

does not describe the data. We have shown for the first time that gray proton production decreases with the total hadronic effective mass, corroborating the model that it is mostly low-energy particles that undergo rescattering.

A significant portion (19%) of the gray proton sample is produced in the backward hemishphere. These particles cannot be produced by a nucleon colliding with a single nucleon target. We searched for evidence that such particles could be produced by secondary collisions off of a cluster of nucleons inside the Neon nucleus. Such effective clusters could be formed due to nuclear density fluctuations, multiquark bags, or the existence of more complex structures in the nucleus such as pairs or triplets of nucleons. A depletion was found in the production of π^+ particles in the momentum range 200-250 MeV/c when there were backward protons in the events, indicating pion absorption. For the first time in a neutrino experiment the following pion absorption mechanisms for backward proton production were studied: $\pi + "b" \rightarrow N + N$ and $\pi + "b" \rightarrow \Delta + N$ with $\Delta \rightarrow \pi + N$, where "b" is assumed to be a two-nucleon system. An analysis of the kinematical variable,

$$\mu^2 \equiv (T_1 + T_2)^2 - (\vec{p}_1 + \vec{p}_2)^2$$

gave evidence for the presence of both processes, with the first one dominating. Effective mass plots of πp combinations were fitted and found to be consistent with 15-20% of the backward protons being produced by Δ^{++} and Δ^0. The mechanism of pion absorption indicates that interactions of slow secondary hadronic matter with other nucleons in the Neon nucleus also contributes to proton production.

The two-nucleon correlation model was further studied for evidence of the neutrino directly interacting with two-nucleon clusters. The model assumes that a two-nucleon cluster is made up of a target nucleon with its momentum vector oriented in the forward direction and a spectator target with equal magnitude of momentum in the opposite direction. When the target nucleon is struck, the backward spectator nucleon is liberated. The variable v_N is thought to decrease with α, as it does in $\nu - D_2$ data. A tendency toward a decrease exists, but it does not agree well with the model.

Invariant differential cross sections for backward particle production confirmed what other experiments have found, namely that the slope B is independent of the particle

type and the hadronic energy. The values of B are consistent with data from other $\nu - Ne$ and $\nu - D_2$ experiments. This distribution may give some evidence for the existence of deuteron-like objects in the Neon nucleus.

Appendix A

(νn) to (νp) Cross Section Ratio

The neutrino-quark cross sections and the quark structure functions can be found in ref.[22], page 274.

$$\frac{d\sigma}{dxdy}(\nu_\mu N \to \mu^- N) = \frac{G^2 xs}{2\pi}(Q(x) + (1-y)^2\bar{Q}(x)) \tag{A.1}$$

$$\propto xQ(x) + x(1-y)^2\bar{Q}(x) \tag{A.2}$$

$$d^p(x) + d^n(x) = d(x) + u(x) \equiv Q(x) \tag{A.3}$$

$$\bar{u}^p(x) + \bar{u}^n(x) = \bar{u}(x) + \bar{d}(x) \equiv \bar{Q}(x) \tag{A.4}$$

u(x) and d(x) are the structure functions of the up and down quarks in a proton. We want to find the ratio of the cross sections of neutrino-neutron to neutrino-proton interactions.

For the neutrino-proton cross section:

$$\frac{d\sigma^{\nu p}}{dxdy} \propto xd(x) + x(1-y)^2\bar{u}(x) \tag{A.5}$$

$$= xd(x) + (1-2y+y^2)x\bar{u}(x) \tag{A.6}$$

$$\frac{d\sigma^{\nu p}}{dx} \propto xd(x) + \frac{1}{3}x\bar{u}(x) \tag{A.7}$$

when we integrate y from 0 to 1. From Field and Feynman, Ref.[21]:

$$\int_0^1 xd(x)dx = 0.145 \tag{A.8}$$

$$\int_0^1 x\bar{u}(x)dx = 0.015 \tag{A.9}$$

$$\sigma^{\nu p} \propto 0.145 + \frac{1}{3}(0.015) = 0.150 \tag{A.10}$$

For the neutrino-neutron cross section:

$$\frac{d\sigma^{\nu n}}{dx\,dy} \propto xu(x) + x(1-y)^2\bar{d}(x) \tag{A.11}$$

$$\frac{d\sigma^{\nu n}}{dx} \propto xu(x) + \frac{1}{3}x\bar{d}(x) \tag{A.12}$$

when we integrate y from 0 to 1. From Field and Feynman:

$$\int_0^1 xu(x)dx = 0.285 \tag{A.13}$$

$$\int_0^1 x\bar{d}(x)dx = 0.021 \tag{A.14}$$

$$\sigma^{\nu n} \propto 0.285 + \frac{1}{3}(0.021) = 0.292 \tag{A.15}$$

So the (νn) to (νp) cross section ratio is:

$$\frac{\sigma^{\nu n}}{\sigma^{\nu p}} = \frac{0.292}{0.150} = 1.95. \tag{A.16}$$

References

[1] W. Busza and R. Ledoux, Ann. Rev. Nucl. Part. Sci. **38**, 119 (1988)

[2] S. Frederickson *et al.*, Phys. Rep. **144**, 187 (1987)

[3] D. H. Brick *et al.*, Phys. Rev. D **39**, 2484 (1989)

[4] V. V. Ammosov *et al.*, Sov. J. Nucl. Phys. **43**, 5 (1986)

[5] M. Dayon *et al.*, Z. Phys. C **56**, 391 (1992)

[6] E. Matsinos *et al.*,Z. Phys. C **44**, 79 (1989)

[7] V. I. Efremenko, Phys. Rev. D **22**, 2581 (1980)

[8] E. B. Brucker *et al.*, Phys. Rev. D **32**, 1605 (1985)

[9] R. D. Amado and R. M. Woloshyn, Phys. Rev. Lett. **36** number 24, 1435 (1976)

[10] D. I. Blokhintsev, Soviet Physics JETP **6**, 995 (1958)

[11] L. L. Frankfurt and M. I. Strikman, Phys. Lett. **69** B number 1, 93 (1977)

[12] R. L. Jaffe, Phys. Rev. Lett. **50**, 228 (1983)

[13] L. Kondratuyk and M. Shmatikov, Z. Phys. A **321**, 301 (1985)

[14] B. S. Yuldashev *et al.*, Phys. Rev. D **46**, 45 (1992)

[15] B. Andersson and I. Otterlund, Nuclear Physics **B99**, 425 (1975)

[16] B. Andersson, I. Otterlund and E. Stenlund, Phys. Rev. B **73**, 343 (1978)

[17] S. Willocq, Ph. D. thesis, Tufts University (1992)

[18] M. Aderholz *et al.*, Phys. Rev. D **45**, 2232 (1992)

[19] D. F. DeProspo, Ph. D. thesis, Rutgers University (1991)

[20] M. K. Hegab and J. Hufner, Nuclear Physics **A384**, 353 (1982)

[21] R. D. Field and R. P. Feynman, Phys. Rev. D **15**, 2590 (1977)

[22] F. Halzen and A. D. Martin, Quarks and Leptons: An Introductory Course in Modern Particle Physics, John Wiley & Sons (1984)

Vita

Mary A. Lauko

1980-1984 B.A. in Physics, Rutgers College at Rutgers, The State University of New Jersey, New Brunswick, New Jersey.

1984-93 Attended The Graduate School at New Brunswick, Rutgers, The State University of New Jersey, New Brunswick, New Jersey.

1984 Tutor in Physics, Department of Physics.

1985 Teaching assistant, Department of Physics.

1986-1988 Course assistant, department advisor in computer grading and department student evaluations, Department of Physics.

1987-93 Research assistant, Department of Physics.

1993 Ph.D. in Physics.